

Multi-Zone Shell Model for Turbulent Wall Bounded Flows

Victor S. L'vov, Anna Pomyalov and Vasil Tiberkevich

Department of Chemical Physics, The Weizmann Institute of Science, Rehovot 76100, Israel

We suggested a *Multi-Zone Shell* (MZS) model for wall-bounded flows accounting for the space inhomogeneity in a “piecewise approximation”, in which cross-section area of the flow, S , is subdivided into “ j -zones”. The area of the first zone, responsible for the core of the flow, $S_1 \simeq S/2$, and areas of the next j -zones, S_j , decrease towards the wall like $S_j \propto 2^{-j}$. In each j -zone the statistics of turbulence is assumed to be space homogeneous and is described by the set of “shell velocities” $u_{nj}(t)$ for turbulent fluctuations of the scale $\propto 2^{-n}$. The MZS-model includes a new set of complex variables, $V_j(t)$, $j = 1, 2, \dots, \infty$, describing the amplitudes of the near wall coherent structures of the scale $s_j \sim 2^{-j}$ and responsible for the mean velocity profile. Suggested MZS-equations of motion for $u_{nj}(t)$ and $V_j(t)$ preserve the actual conservations laws (energy, mechanical and angular momenta), respect the existing symmetries (including Galilean and scale invariance) and account for the type of the non-linearity in the Navier-Stokes equation, dimensional reasoning, etc. The MZS-model qualitatively describes important characteristics of the wall bounded turbulence, e.g., evolution of the mean velocity profile with increasing Reynolds number, $\mathcal{R}e$, from the laminar profile towards the universal logarithmic profile near the flat-plane boundary layer as $\mathcal{R}e \rightarrow \infty$.

PACS numbers: 05.45.-a, 47.27.-i, 47.27.Nz, 47.27.Eq, 47.60.+i

INTRODUCTION

A. Background

Three simple turbulent flows – in a channel, in a pipe and near a flat plane – play a prominent role in our understanding of spatially inhomogeneous wall bounded flows, similar to the celebrative role of the developed homogeneous turbulence in the understanding the universal statistical behavior of fine-scale turbulence. On the long way of understanding homogeneous turbulence there appeared various phenomenological cascade models of turbulence (Richardson-Kolmogorov-41 concept of turbulence, Kolmogorov-62 log-normal and “multi-fractal” models of intermittency), many closure procedures (like Kraichnan Direct Interaction Approximation), various field theoretical approaches. Last but not least we have to mention so-called “shell models” of turbulence (like GOY shell model [1, 2] together with its “Sabra” improvement [3], and many others [4]). Separately we want to mention Zimin’s shell model (V. Zimin, private communication, see also [5, 6]) which has been derived from the Navier-Stokes equation (NSE) using a vector wavelet decomposition [7] of the velocity field, and which involves no empirical or ad hoc parameters.

The shell models are systems of ordinary differential equations which mimic the statistically homogeneous isotropic turbulent velocity field in some interval of scales (say, within some “shell” in the Fourier space) by one or few “shell velocities” $u_n(t)$ [4]. The shell models have the same (quadratic) type of nonlinearity, as the NSE, respect the conservation of energy (in unforced, inviscid limit) and have the build-in “locality” of interaction of neighboring scales, reflecting scale-by-scale energy transfer toward dissipative scales. Surprisingly, the shell models allows to mimic almost everything we know (experimentally, theoretically or by direct numerical simulation)

about highly nontrivial statistics of fine-scale turbulence. This include, for instance, the “intermittent” behavior of the velocity structure functions (which are simultaneous, two-point n th-order correlation function of velocity differences), the fusion rules (which govern asymptotic behavior of many-point velocity correlation functions), and so on. A possible reason for such a lucky success is that the above mentioned (and some other) characteristics of the turbulent statistics are robust and depend only on some very general physical requirements, such as respect of the actual conservation laws, the scale invariance, the type of nonlinearity in the NSE, and the locality of interaction. All these features are accounted for in the shell models.

Unfortunately, the shell models in their traditional formulations describe only the space homogeneous turbulence, leaving aside the wall bounded turbulence, which play a much more important role in practical applications.

Turbulent flows at high Reynolds numbers, $\mathcal{R}e \gg 1$, contain such a wide range of excited lengths and time scales that the direct numerical simulations (DNS) of the NSE are impossible for the foreseeable future. Consequently, practical engineering calculations are based on some model simplifications of NSE, with Reynolds stress models being the most popular approach, see e.g. the book [8], review [9] and references therein. The idea of Osborne Reynolds (see, e.g. Ref. [10]) was to divide the velocity field into the mean flow part $\mathbf{V}(\mathbf{r})$ and the turbulent fluctuating part $\mathbf{u}(\mathbf{r}, t)$ with zero mean and to approximate in some way the hierarchy of equations for various correlation functions (correlators). Equation for $\mathbf{V}(\mathbf{r})$ contains so-called Reynolds stress term, a second order correlator of $\mathbf{u}(\mathbf{r}, t)$. The right hand side (RHS) of equation for the Reynolds stress contains five different terms: the rates of production, dissipation, turbulent transport and viscous diffusion, and the velocity pressure

gradient term. These are one-point, second and third order correlators of velocity and velocity gradients and the pressure-gradient correlator. The equation for only one such object, the dissipation rate, already contains eight correlators up to the 4th order in velocity, which are usually modeled by various closure procedures in terms of the lower order objects. The simplest, old-fashion Millionshchikov's closure (Monin and Yaglom, [10], p. 241) is often invoked. It uses a non-realistic assumption of Gaussian statistics of turbulence. To improve the situation one can use a set of phenomenological constants, which can be found by comparison of the results of model calculations with the results of DNS or experiments in the benchmark flows.

There where attempts to use more advanced field theoretical approaches developed in the theory of homogeneous turbulence, e.g. the Yakhot-Orszag version of the Renormalization Group (RNG) approach [11, 12]. Instead of going into detailed criticism of this approach, already done in Ref. [13], we just make two general remarks to the RNG approach, that are also relevant to the most attempts of a straightforward transfer of the field theoretical methods of fully developed, fine scale, homogeneous turbulence to the case of wall bounded flows. First, in most cases, (RNG, diagrammatic perturbation approach, etc.) the turbulence is assumed to be excited by some artificial external force with Gaussian statistics. This is reasonable simplification of the real picture, if one deals with turbulent scales that are deep enough in the inertial interval. However, this is definitely not a realistic assumption for large scales, that are important in the energy and mechanical momentum balance in wall bounded turbulence. Second, in most cases, the field-theoretical approaches to homogeneous turbulence are usually formulated in the \mathbf{k} -representation or explicitly assumed the space homogeneity. In this way one gets required closure relationships, say between the effective turbulent viscosity ν_T , the density of the kinetic energy \mathcal{E} and the rate of energy dissipation (used in the popular \bar{K} - $\bar{\epsilon}$ version of the Reynolds stress model). However, at least two of these objects (ν_T and \mathcal{E}) are not locally defined, they are dominated by the largest eddies in the system, usually of scales close to the distance to the wall. Therefore one has to be extremely careful applying the resulting relations to the wall bounded flows in which the characteristic length of inhomogeneity is exactly the distance to the wall. A price to pay for such a simplification is that the phenomenological constants may depend on the flow geometry or even on the position in the flow.

Introducing enough adjustable parameters (sometimes geometry dependent), one can reach an engineering goal to model in computer some mean and turbulent characteristics of particular flows of practical importance. However, an important aspects of the basic physics of wall bounded turbulence remain unclear, being masked by numerous details, or even incorrectly reproduced.

The main goal of this paper is to suggest a physically transparent and analytically analyzable model of wall

bounded flows, oriented mainly on physical community. The model describes an interplay of two main physical phenomena in the wall flows: the energy cascade toward small scale (like in the developed homogeneous turbulence) and the cascade of the mechanical momentum toward the wall in the physical space. Our model is a generalization of the shell model of homogeneous turbulence on the case of inhomogeneous turbulence and accounts for a non-uniform profile of the mean velocity. Simplifying assumptions are made from the very beginning, at the level of basic, dynamical equations of motion. These equations involve only two parameters, responsible for the energy and mechanical momentum fluxes. These parameters can be evaluated from the NSE, but currently they are chosen to reproduce the Von Karman constant κ_K and constant B in the universal log-profile of the mean velocity near flat plane.

Our model is oriented toward the classical examples of the wall turbulence, like the channel and the pipe flows, the planar and the circular Couette flows. The physical description of the model and its equations of motion are presented in the following subsection.

B. Multi-zone Shell Model in brief

For dealing with inhomogeneous wall turbulence we suggest in this paper a *piecewise homogeneity approximation* in which the cross-section area of the flow, S , is subdivided into a set of " j -zones". The area of the first zone, responsible for the core of the flow, $S_1 \approx S/2$, and the areas of the next j -zones, S_j , decrease towards the wall like $S_j \propto 2^{-j}$. In each j -zone, the statistics of turbulence is assumed to be space homogeneous and is described by its own shell model

$$\frac{du_{nj}(t)}{dt} = -\nu_n \kappa_n^2 u_{nj} + \mathcal{N}_{nj} + \Delta_{nj} w_n, \quad (0.1)$$

for the "shell velocities" $u_{nj}(t)$, which are responsible for turbulent fluctuations of the (dimensionless) scale $s_n \sim 2^{-n}$, referred for below as (nj) -eddies. Hereafter Δ_{nj} is the Kronicker symbol ($= 1$ for $n = j$ and $= 0$ otherwise). Equation (0.1) accounts for the viscous damping term with some effective viscosity $\nu_n \sim \nu_0$, where ν_0 is the kinematic viscosity of the fluid. The effective "shell" wave vector $\kappa_n \propto 1/s_n$. The nonlinear term in Eq. (0.1), \mathcal{N}_{nj} , is given by Eq. (1.17) and describes the usual triad interaction of nearest shells, inside of a given j -zone, Eq. (1.13), and some inter-zone interaction term of similar type. The production term w_n is responsible for the energy flux from the mean flow to the turbulent subsystem and is given below by Eq. (2.39).

Our goal is to describe the mean velocity profile $\langle \mathbf{V}(\rho, t) \rangle$, in which ρ is two dimensional radius-vector in the cross-section of the flow, $\rho \perp \hat{\mathbf{x}}$, $\hat{\mathbf{x}}$ is the streamwise direction. To this end we introduce additional variables $V_j(t)$ with a prescribed space dependence $\Phi_j(\rho)$,

uniquely determined by the flow geometry. The variables $V_j(t)$ can be understood as complex amplitudes of the near-wall coherent structures of the dimensionless scale s_j , which is the same, as the scale of (nj) -eddies: $s_j = h_n$ for $n = j$. The functions $\Phi_j(\rho)$ are chosen such that $\Phi_{j+1}(\rho) \simeq \Phi_j(2\rho)$ and form an orthonormal, (but incomplete) basis. We call it “*PM-basis*”, because (in spite of its incompleteness) it is chosen such as to represent *exactly* the densities of the mechanical linear and angular momenta, \mathcal{P} and \mathcal{M} , in terms of $V_j(t)$ only:

$$\mathcal{P} = \sum_j s_j \operatorname{Re}[V_j(t)], \quad \mathcal{M} = \sum_j s_j R_j \operatorname{Im}[V_j(t)]. \quad (0.2)$$

Here R_j is the characteristic distance of the j -zone from the centerline of the flow. The *PM-basis* also allows one to reconstruct the spatial dependence of the mean flow (and its time depending fluctuations) with a finite (but very good) accuracy

$$\mathbf{V}(\rho, t) \approx \mathbf{V}_{\text{PM}}(\rho, t) \equiv \operatorname{Re} \left[\sum_j V_j(t) \Phi_j(\rho) \right]. \quad (0.3)$$

For the *PM-velocities* $V_j(t)$ we suggest a simple *momentum equation*

$$\frac{dV_j(t)}{dt} = -\nu_j \kappa_j^2 V_j + \nabla p + W_j, \quad (0.4)$$

which includes the viscous term, $\nu_j \kappa_j^2 V_j$, pressure gradient, $\nabla p > 0$, and the Reynolds stress term, W_j , that accounts for the exchange of the mechanical momentum between nearest zones in the flow and is given by Eq. (2.38).

It is crucially important that suggested *multi-zone shell model*, Eqs. (0.1) and (0.4), preserves (in the unforced, inviscid limit) all the relevant in the problem integrals of motion: energy, \mathcal{E} , mechanical momenta, \mathcal{P} and \mathcal{M} .

C. The plan of the paper

Section I is devoted to the statistical description of the “turbulent part” of the Multi-Zone Shell model (MZS-model), Eq. (0.1). First, in Sec. IA we describe a way from the NSE to a standard shell model of homogeneous turbulence, that allows generalization for space inhomogeneous turbulence. Next, in Sec. IB we formulate a piece-wise homogeneity approximation: the cross-section area of the flow, S , is subdivided into set of “ j -zones”, in each of them the statistics of turbulence is assumed to be space homogeneous. This allows us to use the standard shell model for every j -zone and to describe the turbulence in the whole flow by the set of “shell velocities” $u_{nj}(t)$ for turbulent fluctuations of the scale $\propto 1/2^n$.

In Sec. II we derive the dynamical equation of motion for the so-called *PM-velocities*, V_j , that allows one to reconstruct with good accuracy the mean velocity profile $\mathbf{V}(\rho)$ in the cross-section of the flow. In particular,

in Sec. IIB we introduce the *PM-basis* for a wide class of wall bounded flows that connects $\mathbf{V}(\rho)$ and V_j . In Sec. IIC we derive Eq. (0.4) for V_j and for all involved in Eq. (0.4) terms.

In Section III we discuss the conservation laws (Sec. III B) and the symmetries (Sects. III C and III D) of the MZS model. For the convenience of the reader it begins with the overview of the resulting MZS equations, presenting them, in Sec. III A, in the dimensionless form (3.3), convenient for the further analysis. In particular, we derive in Sec. III D the version of the MZS model for the turbulent boundary layer near flat plane, Eqs. (3.19).

Section IV presents a detailed analytical study of the MZS equations in a set of approximations, realistic at various values of \mathcal{Re} . In Sec. IV A we show that the MZS-model describes the stable laminar velocity profile for small \mathcal{Re} and its instability at some threshold value of $\mathcal{Re} = \mathcal{Re}_{\text{cr}}$. Next, in Sec. IV B we study the MZS-model in the approximation of the near-wall eddies, neglecting the turbulent energy cascade. This effect is accounted for in Sec. IV C in the approximation of turbulent viscosity. Section IV D is devoted to numerical analysis of the MZS-model.

In Section V, we summarize our findings and suggest a possible generalization of the model for the description of turbulent flows laden with the long-chain polymeric additives (in connection with the problem of drag reduction) or with heavy micro-particles, etc.

1. Some notations and definitions

- $\hat{\mathbf{x}}$ & ρ – the streamwise direction & the two-dimensional radius-vector in the cross-section of a flow, $\rho \perp \hat{\mathbf{x}}$. In a channel $\rho = (y, z)$, with y as the wall-normal and z as the spanwise directions.

- S_{\perp} , P_{\perp} & L – the cross-section area, the perimeter and the characteristic length of a cross-section:

$$S_{\perp} = \int d\rho, \quad L \equiv S_{\perp}/P_{\perp}. \quad (0.5)$$

In a channel of width $2H$, $L = H$; in a pipe of radius R , $L = R/2$.

- ∇p – the external pressure gradient, that is a positive constant

$$\nabla p \equiv -\frac{dp(x)}{dx} > 0. \quad (0.6)$$

- τ & U_{τ} – the characteristic time & the velocity in the flow:

$$\tau \equiv \sqrt{L/\nabla p}, \quad U_{\tau} \equiv \sqrt{L\nabla p}. \quad (0.7)$$

The wall shear stress is U_{τ}^2 .

- ν_0 & \mathcal{Re} – the kinematic viscosity & the friction Reynolds number

$$\mathcal{Re} \equiv U_{\tau} L / \nu_0. \quad (0.8)$$

- f' & f'' – the real and imaginary parts of some complex object f (constant, variable, function, etc.):

$$f' \equiv \text{Re}\{f\}, \quad f'' \equiv \text{Im}\{f\}. \quad (0.9)$$

- n , j & p are dummy indices (natural numbers), reserved for the scale (or shell), zone & position indices; some objects can be related both to the shells and zones. They are used with both n or j indices.

- s_j & σ_j – the fraction of the cross-section area, occupied by the j -zone, & the fraction of the cross-section area occupied by all zones towards the wall, starting from the zone j :

$$s_j \equiv \frac{S_j}{S_\perp}, \quad \sigma_j \equiv \sum_{i=j}^{\infty} s_i, \quad \sigma_1 = \sum_{j=1}^{\infty} s_j = 1. \quad (0.10)$$

- $L_j \equiv s_j L$ – the width of the j -zone, L_n – the characteristic scale in the n -shell
- $\kappa_n \equiv 1/(2L_n)$ – the wave number in the n -shell; κ_j – the wave number of the j -zone
- \mathcal{E} , \mathcal{P} , & \mathcal{M} – the densities of the energy, of the mechanical linear & angular momenta ($\hat{\mathbf{x}}$ projections)
- ε^\pm , \mathfrak{p}^\pm , & \mathfrak{m}^\pm – the total rates of pumping (with $+$) and dissipation (with $-$) of the conserved quantities \mathcal{E} , \mathcal{P} , & \mathcal{M}
- ε_j^\pm , \mathfrak{p}_j^\pm , & \mathfrak{m}_j^\pm – the rates of pumping (with $+$) and dissipation (with $-$) in the j -zone (of \mathcal{E} , \mathcal{P} , & \mathcal{M})
- ε_j , \mathfrak{p}_j , & \mathfrak{m}_j – the fluxes of \mathcal{E} , \mathcal{P} , & \mathcal{M} from the j - to the $(j+1)$ -zone
- The scalar product of complex vector functions, $\mathbf{A}(\rho)$ & $\mathbf{B}(\rho)$:

$$(\mathbf{A}, \mathbf{B}) \equiv \int \mathbf{A}^*(\rho) \cdot \mathbf{B}(\rho) \frac{d\rho}{S_\perp}. \quad (0.11)$$

- $\phi_m^+(\rho)$ & $\phi_m^-(\rho)$ the even and odd eigenfunctions of the two-dimensional Laplace operator in the cross-section of the flow with no-slip boundary conditions, $\phi_m^\pm(-\rho) = \pm \phi_m^\pm(\rho)$
- $\Phi_j(\rho) = \Phi'_j(\rho) + i\Phi''_j(\rho)$ – PM -basis functions, Eq. (2.4)
- $V_{PM}(\rho)$ & V_j – PM -velocity in the coordinate and j -representations, related by Eq. (2.14)
- u_{nj} – the velocity of turbulent fluctuation of the scale $\propto 2^{-n}$ in the j -zone [(nj)-eddies]; $u_j \equiv u_{jj}$

I. STATISTICAL MULTI-ZONE SHELL MODEL FOR TURBULENT FLUCTUATIONS

A. From NSE to shell models of homogeneous turbulence

In this Subsection we present a re-derivation of a standard shell model of space homogeneous turbulence in a way that allows us to generalize it in Sec. I B for the case of space inhomogeneity.

1. “Cell basis”, wavelets and “(np)-eddies”

Consider for simplicity an incompressible turbulent velocity $\mathbf{u}(\mathbf{r}, t)$ in a periodic box of size $L \times L \times L$. Instead of the \mathbf{r} - or \mathbf{k} -representation we introduce here a “cell basis” $\Psi_{np}(\mathbf{r})$, which is quite similar to wavelet bases (for an easy-to-read, introductory text about the theory of wavelets see, e.g. [14]). Similar to the wavelet bases, the cell bases reflect both spatial scales of turbulent structures (like in the \mathbf{k} -representation) and their position in the physical space (like \mathbf{r} -representation) but accounts for the actual boundary conditions of the flow. The *cell index*, (n, \mathbf{p}) , consists of the *scale index* $n = 1, 2, \dots \infty$ and the *position index* $\mathbf{p} = (p_x, p_y, p_z)$:

The *scale index* $n = 1, 2, \dots \infty$ defines the characteristic width L_n (in all directions) of the function $\Psi_{np}(\mathbf{r})$, which some “(np)-cell” of the size $L_n = L/2^n$ “occupies” in space.

The *position index* $\mathbf{p} = (p_x, p_y, p_z)$ defines the position \mathbf{R}_{np} of the (np)-cell:

$$\mathbf{R}_{np} \equiv \mathbf{p} L_n, \quad \mathbf{p} = (p_x, p_y, p_z), \quad (1.1) \\ \mathbf{p} \in \mathcal{C}_n \Leftrightarrow p_\alpha = 1, 2, \dots 2^n, \quad \alpha = x, y, z.$$

One can imagine that, for any given n , the set of (np)-cells with $\mathbf{p} \in \mathcal{C}_n$ fills the periodical L^3 -box. The turbulent velocity field $\mathbf{u}(\mathbf{r}, t)$ is given by:

$$\mathbf{u}(\mathbf{r}, t) = \sum_{n=1}^{\infty} \sum_{\mathbf{p} \in \mathcal{C}_n} \text{Re}\{U_{np}(t)\Psi_{np}(\mathbf{r})\}, \quad (1.2)$$

where the amplitude of the “cell expansion”, $U_{np}(t)$ is the velocity difference across the separation L_n in the (np)-cell.

It is convenient to normalize the cell-basis as follows:

$$\iiint_{000}^{LLL} \Psi_{np}^*(\mathbf{r}) \cdot \Psi_{n'p'}(\mathbf{r}) \frac{dxdydz}{L^3} = 2v_n \Delta_{nn'} \Delta_{pp'}, \\ \iiint_{000}^{LLL} \Psi_{np}(\mathbf{r}) \cdot \Psi_{n'p'}(\mathbf{r}) \frac{dxdydz}{L^3} = 0. \quad (1.3a)$$

Here $v_n = 2^{-3n}$ is the dimensionless part of the total volume per one mode in the n th cell.

The equations (1.2) and (1.3) give the Parseval identity for the density of the turbulent energy in the form:

$$\mathcal{E} \equiv \iiint_{000}^{LLL} \frac{|\mathbf{u}(\mathbf{r}, t)|^2}{2} \frac{dxdydz}{L^3} = \sum_{n=1}^{\infty} \mathcal{E}_n(t), \quad (1.4a)$$

$$\mathcal{E}_n(t) = v_n \sum_{\mathbf{p} \in \mathcal{C}_n} \frac{|U_{np}(t)|^2}{2}. \quad (1.4b)$$

This equation supports our interpretation of $U_{np}(t)$ as the velocity difference across the separation L_n in the

(np)-cell. We will refer to these fluctuations as to “(np)-eddy”.

A particular choice of the cell functions $\Psi_{np}(\mathbf{r})$ is not important for us here. Notice only, that for large n basic cell functions become scale invariant and may be obtained by dilatations of one (or few) n -independent function $\Psi_\infty(x)$. In this limit the cell basis becomes the wavelet one with $\Psi_\infty(x)$ as so-called “ \mathcal{R} -wavelet” [14]. An explicit example of a divergence-free 3 dimensional vector \mathcal{R} -wavelet function given in [5].

The cell functions $\Psi_{np}(\mathbf{r})$ form a complete orthonormal basis, therefore one can derive the *exact equation of motion* for $U_{np}(t)$ by the Galerkin projection of NSE:

$$\begin{aligned} \frac{dU_{np}^\sigma(t)}{dt} &= - \sum_{\mathbf{p}'} \Gamma_{n,\mathbf{p}\mathbf{p}'} U_{np'}^\sigma(t) \quad (1.5) \\ &+ \sum_{n'n''} \sum_{\mathbf{p}'\mathbf{p}''} \sum_{\sigma'\sigma''=\pm} T_{nn'n'',\mathbf{p}\mathbf{p}''}^{\sigma'\sigma''} U_{n'\mathbf{p}'}^{\sigma'}(t) U_{n''\mathbf{p}''}^{\sigma''}(t), \end{aligned}$$

where $\sigma, \sigma', \sigma'' = \pm$ are sign indices and we accept the convention $U_{np}^- \equiv U_{np}$ and $U_{np}^+ \equiv U_{np}^*$. The explicit forms of the damping parameters Γ and amplitudes T depend on the basis, see, e.g. [5].

2. Basic assumptions for the standard shell models

Consider shortly the physical simplifications that allows one to reduce the NSE to the shell model of homogeneous turbulence. Unlike the similar discussion in [5], we made an accent on the assumption of space homogeneity and the possibility to relax this assumption in order to generalize shell models for the space inhomogeneous case.

The standard shell models of homogeneous turbulence follow from the exact Eq. (1.5) with the following simplifying assumption of a *statistical nature*:

$$U_{np}(t) \Rightarrow u_n(t) A_{np}, \quad (1.6a)$$

$$\overline{A_{np}} = 0, \quad \overline{|A_{np}|^2} = 1. \quad (1.6b)$$

Here A_{np} are *time independent*, random amplitudes, and $\overline{\quad}$ denotes averaging over yet unknown statistics of A_{np} , which is generated by the NSE (1.5). The physical meaning of $u_n(t)$ is the mean square velocity *fluctuations* of all (np)-eddies :

$$\overline{\langle |U_{np}(t)|^2 \rangle} = \langle |u_n(t)|^2 \rangle, \quad (1.7)$$

with the mean velocity equal to zero $\overline{\langle U_{np}(t) \rangle} = 0$, even if the time averaged shell velocity $\langle u_n(t) \rangle \neq 0$.

The physical arguments behind Eq. (1.6) may be based on the fact that in the homogeneous turbulence all velocities $U_{np}(t)$ with different \mathbf{p} have the same statistics. Eq. (1.6) therefore neglects only the difference between the *actual time realizations* of np -velocities $U_{np}(t)$ of the

same scale (the same scale index n), but occupying different cells (different position index \mathbf{p}). The ensemble of the time realizations is replaced by the time-independent ensemble of A_{np} . With the assumption (1.6), Eq. (1.5) yields:

$$\frac{du_n(t)}{dt} = -\gamma_n u_n(t) + N_n, \quad (1.8a)$$

$$\gamma_n = \sum_{\mathbf{p}'} \Gamma_{n,\mathbf{p}\mathbf{p}'} \overline{A_{np} A_{np'}}, \quad (1.8b)$$

$$N_n = \sum_{n'n'', \sigma'\sigma''} S_{nn'n'', \mathbf{p}\mathbf{p}'}^{\sigma'\sigma''} u_{n'}^{\sigma'}(t) u_{n''}^{\sigma''}(t), \quad (1.8c)$$

$$S_{nn'n''}^{\sigma'\sigma''} = \sum_{\mathbf{p}'\mathbf{p}''} T_{nn'n'', \mathbf{p}\mathbf{p}''}^{\sigma'\sigma''} \overline{A_{np} A_{n'\mathbf{p}'} A_{n''\mathbf{p}''}}. \quad (1.8d)$$

The correlation functions of A_{np} can be evaluated with some reasonable *statistical* assumptions (for instance, with some closure procedure, like Direct Interaction Approximation, see e.g. [5]).

Under assumption (1.6), Eq. (1.4b) gives a usual equation for the density of the total energy of the n th scale: $\mathcal{E}_n(t) = \frac{1}{2} |u_n(t)|^2$. Different shell models correspond to various further simplifications of the nonlinear term (1.8c). For example, in the Sabra shell model [3]:

$$N_n = i [a \kappa_{n+1} u_{n+1}^* u_{n+2} + b \kappa_n u_{n-1}^* u_{n+1} - c \kappa_{n-1} u_{n-2} u_{n-1}], \quad (1.9a)$$

$$\kappa_n \propto 2^n, \quad a + b + c = 0. \quad (1.9b)$$

Notice, that the scale index n in the Eqs. (1.8) and (1.9) for shell models becomes the *shell index*.

B. Piece-wise homogeneity approximation and multi-zone shell model for turbulent fluctuations

The turbulent fluctuations in the wall bounded flows are not space homogeneous due to the spatial dependence of the mean velocity profile, which, in its turn, is also affected by the turbulent fluctuations. Due to the inhomogeneity of turbulence, the shell model approach discussed in Sec. IA have to be revised, which is the subject of this subsection. For concreteness we discuss the planar geometry of the channel flow of width $2H$ in the cross-stream direction y , see Fig. 1. In further analysis we consider only the low half of the channel, $0 < y < H$, having in mind that the flow in the second half of the channel, $H < y < 2H$, is statistically identical to the that in the first one.

Clearly, the core of the flow (say, for $H/2 < y < H$) may be approximately viewed as homogeneous. Let us call this region the “1-zone”. The next region $H/4 < y < H/2$, in which the mean velocity profile $V(y)$ begin to decrease towards the wall, we call the “2-zone”. Notice, that the width of the 2-zone, $H_2 = H/4$ is a half of the 1-zone width, $H_1 = H/2$. Therefore, approximately with the same accuracy we can consider the statistics of

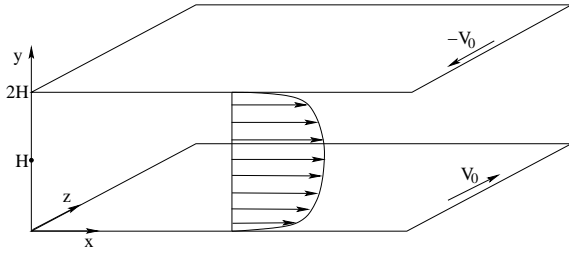


FIG. 1: Geometry of the channel and the plane Couette flow between two parallel planes separated by $2H$ in the cross-stream direction y . In the simple channel flow the pressure gradient is applied in the “streamwise” direction x and the mean velocity $\bar{V}(y)$ is oriented also along x . In the plane Couette flow the lower wall ($y = 0$) is moving in z (spanwise) direction with some velocity V_0 , while the upper wall ($y = 2H$) is moving in the opposite direction. In this case $\bar{V}(y)$ has z -projection. For both flows (and their hybridization) the three-dimensional velocity fluctuations are space-homogeneous in the $x - z$ plane.

turbulence in the 2-zone as homogeneous, but different from that in the 1-zone.

Similarly, one expects that the mean velocity difference across each next j -zone of the width $H_j = H/2^j$ will be more or less the same. This is the motivation to define “ j -zone” in the scale invariant manner, as $2^{-j}H < y < 2^{-(j-1)}H$ and to approximate the turbulence inside each such zone as homogeneous.

The approximation of the piecewise homogeneity allows one to use the shell-model reduction, Eq. (1.6), inside of each j -zone, similarly to that in the whole space for homogeneous turbulence:

$$U_{n\mathbf{p}}(t) \Rightarrow u_{nj}(t)A_{n\mathbf{p}_j}, \quad 1 \leq j \leq n, \quad (1.10a)$$

$$\begin{aligned} \overline{A_{n\mathbf{p}}} &= 0, & \overline{|A_{n\mathbf{p}}|^2} &= 1, \\ u_{nj} &= u_{nn}, & j > n. \end{aligned} \quad (1.10b)$$

Here \mathbf{p}_j belong to the j -zone, in the sense that the $(n\mathbf{p}_j)$ -cells are inside the j -zone. We introduced in Eq. (1.10a) the velocity of (nj) -eddies, n th shell in the j -zone. Equation (1.10b) reflects the fact that the near-wall (nj) -eddies with zone index $j > n$ belong simultaneously to the j -zone with $j = n$, see Fig. 2. Therefore in our model all $u_{nj}(t)$ with $j > n$ are just $u_{nn}(t)$.

With Eqs. (1.10) one gets from Eqs. (1.4b):

$$\mathcal{E}_n(t) = \sum_{j=1}^{\infty} \frac{H_j}{H} \mathcal{E}_{nj}(t), \quad \mathcal{E}_{nj}(t) = \frac{|u_{nj}(t)|^2}{2}, \quad (1.11)$$

where \mathcal{E}_{nj} is the energy density of the n th shell in the j -zone of the width $H_j = H/2^j$.

Using Eqs. (1.10) and (1.5) one gets the equation of motion of the multi-zone shell model for turbulent fluctuations:

$$\frac{du_{nj}(t)}{dt} = -\gamma_n u_{nj}(t) + \mathcal{N}_{nj} + \Delta_{nj} w_j, \quad (1.12)$$

in which we have added by hand the production term w_j , describing the energy pumping to the turbulent system. This term will be clarified in the following Section by Eq. (2.39).

The nonlinear term \mathcal{N}_{nj} in Eq. (1.12) describes the total energy balance for the n th shell in the j -zone. There are two distinct geometries: $j < n$ and $j \geq n$. In the latter case it is enough to describe the energy balance for $j = n$, since all $u_{nj} = u_{nn}$ for $j > n$.

All eddies with $j < n$ are fully placed in the same zone (e.g., the eddies of shells $n = 2, 3$ and 4 , that belong to the 1st zone, see Fig. 2). Therefore in this case we can use for $\mathcal{N}_{nj}(t)$ a standard shell model expression for N_n , in which $u_{nj} \Rightarrow u_n$. In this paper we adopt the Sabra version of N_{nj} term, generalizing Eq. (1.9):

$$\mathcal{N}_{nj}(t) = N_{nj}(t), \quad \text{for } j < n, \quad (1.13a)$$

$$\begin{aligned} N_{nj} &= i[a \kappa_{n+1} u_{n+1,j}^* u_{n+2,j} \\ &+ b \kappa_n u_{n-1,j}^* u_{n+1,j} - c \kappa_{n-1} u_{n-2,j} u_{n-1,j}]. \end{aligned} \quad (1.13b)$$

The energy balance of the near-wall eddies ($n = j$) is quite different. As one sees in Fig. 2 (on the example of the eddy in the first shell), the near-wall eddies participate in the triad interactions of three types:

- *Triad 1* involves one near-wall eddy and two bulk eddies $[(u_{11} - u_{21} - u_{31})$ triad of the 1st-zone in the above example]. For this interactions we will use Eq. (1.9) but with different parameters: a_1, b_1 and c_1 ;
- *Triad 2* involves two near-wall eddies and one bulk eddy $[(u_{12} - u_{22} - u_{32})$ triad of the 2st-zone in Fig. 2]. Here we will use Eq. (1.9) with the parameters: a_2, b_2 and c_2 ;
- *Triad 3* involves three near-wall eddies $[(u_{13} - u_{23} - u_{33})$ triad of the 3rd-zone in the above example]. Here we will use again Eq. (1.9) with the parameters: a_3, b_3 and c_3 .

The relationships between four set of interaction parameters $[(a, b, c)$ and (a_p, b_p, c_p) , $p = 1, 2, 3$] may be found from: i) the requirement of the conservation of energy and ii) the “correspondence principle”:

For the space homogeneous case (u_{nj} is independent of the zone index j) the multi-zone model must coincide with the usual shell model for homogeneous turbulence (in our case, with the Sabra model).

The above two requirements give:

$$a_1 = a/2, \quad a_2 = a_3 = a/4, \quad (1.14)$$

$$b_1 = b, \quad b_2 = b_3 = b/2,$$

$$c = c_1 = c_2 = c_3.$$

These equations may be interpreted as follows:

- in the *Triads 1* only the half of the largest eddy belongs to the same zone as two smaller ones. This gives $a_1 = a/2$. Two smaller eddies in the *Triad 1* fully belong to their zone. This corresponds to $b_1 = b$ and $c_1 = c$;
- in the *Triads 2* only the quarter of the largest eddy belongs to the same zone as two smaller ones. Therefore $a_2 = a/4$. In this triad only the half of the middle eddy belongs to the same zone as the smallest one. This corresponds to $b_2 = b/2$. The smallest eddy in the triad fully

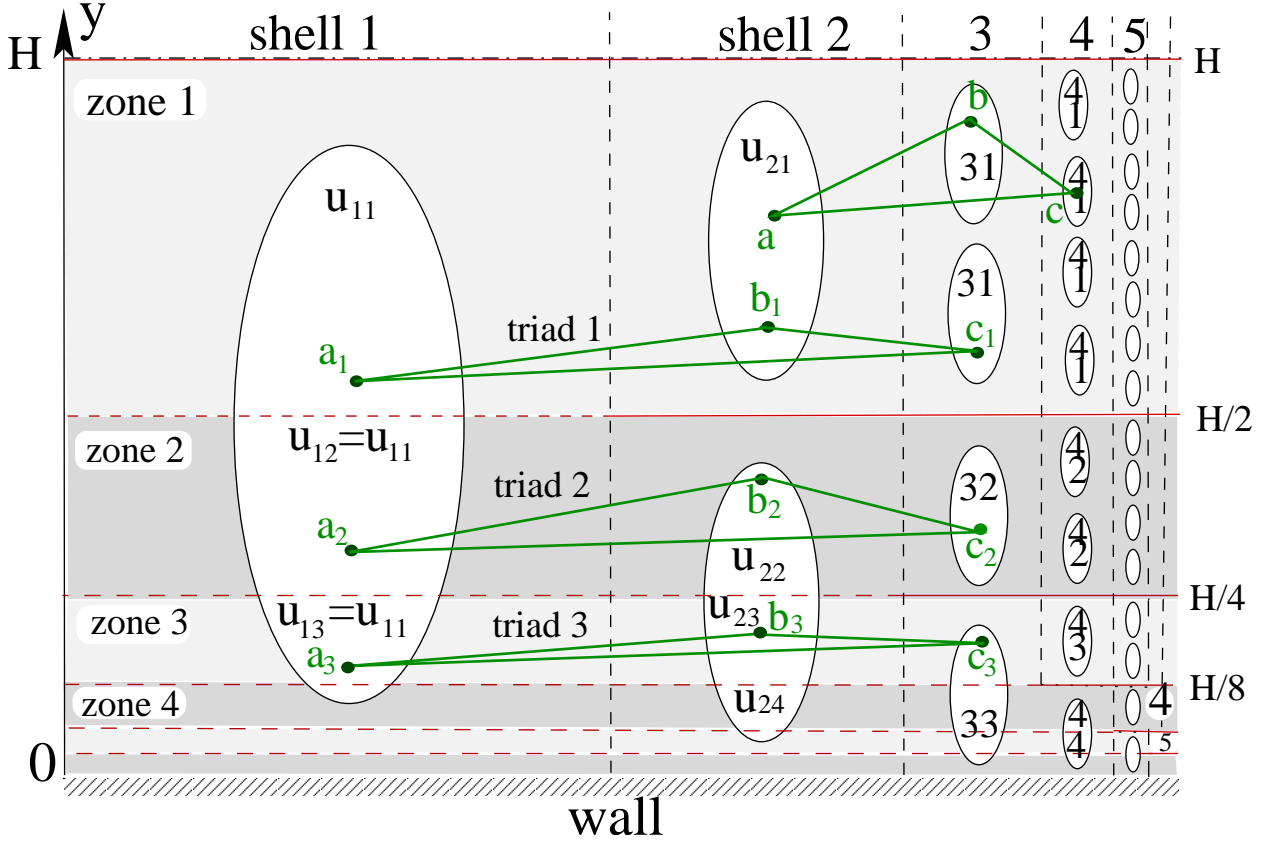


FIG. 2: Zones, shells and triad interactions in the multi-zone shell model for the channel geometry. Regions of localization of (np) -eddies are shown schematically as ellipses with corresponding numbers inside. The near-wall eddies have $n = j$. They also occupy all j -zones towards the wall, with $j > n$.

belongs to their own zone, and we take $c_2 = c$;
– in the *Triads 3* only the quarter of the largest eddy, the half of the middle one and the full smallest eddy belong to the same set of zones (Zones 3,4,.. in our example). This corresponds to the relationships $a_3 = a/4$, $b_3 = b/2$ and $c_3 = c$.

The total contribution of three types of the triad interactions to the nonlinearity of the near-wall eddies can be summarized as follows:

$$\mathcal{N}_{nn} = \frac{1}{4} [2N_{n,n} + N_{n,n+1} + N_{n,n+2}] . \quad (1.15)$$

One can join two Eqs. (1.13) and (1.15) and write:

$$\begin{aligned} \mathcal{N}_{nj} = N_{nj} + \Delta_{nj} \left[\frac{1}{4} (N_{n,n+1} - N_{nn}) \right. \\ \left. + \frac{1}{4} (N_{n,n+2} - N_{nn}) \right] . \end{aligned} \quad (1.16)$$

Obviously, in the homogeneous case the second term in the RHS of Eq. (1.16) vanishes and one recovers the usual shell model for homogeneous turbulence with $\mathcal{N}_{nj} \Rightarrow N_n$.

Notice that the explicit form of this equation reflects the fact that we have accounted only for the triad interactions involving the nearest shells ($n - 1$, n and $n + 1$) and the particular form of the channel subdivision on the

zones: $H_j = 2^{-j}H$. This subdivision of the cross-section area on zones is reasonable for the scale invariant case of turbulent boundary layer near flat plane. The physically motivated subdivision in particular flow geometries will be discussed in the following section. In general case Eq. (1.15) is changed as follows:

$$\begin{aligned} \mathcal{N}_{nj} &= N_{nj} + \Delta_{nj} \sum_{i=n+1}^{\infty} \frac{s_i}{\sigma_j} (N_{ni} - N_{nn}) , \quad (1.17) \\ \sigma_j &\equiv \sum_{i=j}^{\infty} s_i , \end{aligned}$$

with an arbitrary dependence of the (dimensionless) j -zone areas, s_j , on j and an arbitrary form the nonlinear term N_{nj} . The fact that under the sum one has the difference $(N_{nj} - N_{nn})$ guarantees the correspondence principle, while the weights s_i/σ_j follow from the requirement of the conservation of the total energy, which in the case of arbitrary zone division is given by a natural generalization of (1.11) with H_j/H replaced by s_j :

$$\mathcal{E}_n(t) = \sum_{j=1}^{\infty} s_j \mathcal{E}_{nj}(t) , \quad \mathcal{E}_{nj}(t) = \frac{|u_{nj}(t)|^2}{2} . \quad (1.18)$$

II. DYNAMICAL MULTI-SCALE MODEL FOR THE “PM-VELOCITY”

A. Mechanical momenta, \mathbf{P} and \mathbf{M} , and “statistics vs. dynamics” dilemma

The unbounded turbulence may be described in the reference system with a zero mean velocity. In that system the total linear momentum vanishes: $\mathbf{P} = 0$. Due to the Galilean invariance the space homogeneous velocity does not interact with the turbulent fluctuations. Therefore one can consider turbulence in any other reference system with $\mathbf{P} \neq 0$ with the same result for the statistic of turbulence. Hence, the mechanical momentum is not a relevant integral of motion for the unbounded turbulence. This is not the case for the wall bounded turbulence, in which the Galilean invariance is broken by the presence of the walls. The conservation laws for the total linear momentum, \mathbf{P} , (as well as for the total angular momentum, \mathbf{M}) give an important constraint on the expected behavior of the system. For example, in the channel and pipe flows, the total input of the linear momentum due to the pressure gradient, acting in the whole cross-section area of the flow, must be equal to the dissipation of the momentum on the walls due to the viscous friction. Clearly, an analytical description of the wall bounded turbulence must respect the conservation of \mathbf{P} and \mathbf{M} (in the unforced, inviscid limit).

Consider the mean velocity field $\mathbf{V}(\boldsymbol{\rho})$ in the simple flows with translation symmetry in the streamwise direction $\hat{\mathbf{x}} \parallel \mathbf{P}$, in which also $\mathbf{M} \parallel \hat{\mathbf{x}}$. Here $\boldsymbol{\rho}$ is the radius-vector in the cross-section of the flow, $\boldsymbol{\rho} \perp \hat{\mathbf{x}}$. The examples of such flows are the channel and the pipe flows, the planar Couette flow, Fig. 1, the circular Couette flow, etc. Instead of \mathbf{P} and \mathbf{M} , it is more convenient to deal with their volume densities \mathcal{P} and \mathcal{M} , defined as follows:

$$\mathcal{P} = \mathcal{P}_x = (\hat{\mathbf{x}}, \mathbf{V}), \quad (2.1a)$$

$$\mathcal{M} = \mathcal{M}_x = (\mathbf{R}, \mathbf{V}), \quad \mathbf{R} \equiv \hat{\mathbf{x}} \times \boldsymbol{\rho} \quad (2.1b)$$

where (\mathbf{A}, \mathbf{B}) is the scalar product (0.11).

Our idea is to divide the full velocity field $\mathbf{V}(\boldsymbol{\rho})$ into two parts, denoted as $\mathbf{V}_{PM}(\boldsymbol{\rho})$ and $\mathbf{V}_T(\boldsymbol{\rho})$, such that the “turbulent part” $\mathbf{V}_T(\boldsymbol{\rho})$ does not contribute to \mathcal{P} and \mathcal{M} :

$$(\hat{\mathbf{x}}, \mathbf{V}_T) = 0, \quad (\mathbf{R}, \mathbf{V}_T) = 0, \quad (2.2)$$

and to take a special care only on $\mathbf{V}_{PM}(\boldsymbol{\rho})$ part, contributing to \mathcal{P} and \mathcal{M} . This division may be done in many ways, our particular choice will be clarified below by Eq. (2.14).

The description of $\mathbf{V}_{PM}(\boldsymbol{\rho}, t)$ may be statistical or dynamical. The statistical description is the straightforward “cell-expansion approach to shell models”, based on the NSE for $\mathbf{V}_{PM}(\boldsymbol{\rho}, t)$ in the cell representation, similar to Eq. (1.5). To continue, one has to find some reasonable statistical simplifications, similar to Eq. (1.10). However, since of $\mathcal{P} \neq 0$ and/or $\mathcal{M} \neq 0$, now also $\langle \mathbf{V}_{PM}(\boldsymbol{\rho}, t) \rangle \neq 0$ and therefore $\overline{A_{np}}$ cannot be approximated as zero. This

makes it hardly possible to remain on the level of statistical description and one has to deal with the detailed, dynamical description of the *PM-velocity* $\mathbf{V}_{PM}(\boldsymbol{\rho}, t)$ in terms of the NSE. This is the subject of the following Subsections.

B. PM-basis, properties and interpretation

1. Construction of the PM-basis

To construct a “physically motivated” basis for description of the *PM-velocities*, consider two subsets of eigenfunctions of the Laplace operator, $\phi_m^+(\boldsymbol{\rho})$ and $\phi_m^-(\boldsymbol{\rho})$, satisfying the incompressibility condition. The no-slip boundary conditions are assumed in the cross-section of the flow, with the constraints

$$p_m = (\hat{\mathbf{x}}, \phi_m^+) \neq 0, \quad (2.3a)$$

$$\mathcal{R}_m = (\mathbf{R}, \phi_m^-) \neq 0, \quad (2.3b)$$

dictated by Eq. (2.2). Notice that both sets ϕ_m^+ and ϕ_m^- are chosen here as real and orthonormal.

Introduce the complex *PM-basis* as follows:

$$\Phi_j(\boldsymbol{\rho}) = \sum_{m \in \mathcal{S}_j} \left[p_m \phi_m^+ - i \frac{\mathcal{R}_m}{R_j} \phi_m^- \right], \quad (2.4a)$$

$$m \in \mathcal{S}_j \Leftrightarrow 2^{j-1} \leq m \leq 2^j - 1. \quad (2.4b)$$

The normalization “radius” R_j , is chosen such that

$$(\Phi'_j, \Phi'_j) = (\Phi''_j, \Phi''_j), \quad (2.5)$$

where

$$\Phi'_j(\boldsymbol{\rho}) \equiv \text{Re}[\Phi_j(\boldsymbol{\rho})], \quad \Phi''_j(\boldsymbol{\rho}) \equiv \text{Im}[\Phi_j(\boldsymbol{\rho})].$$

Denote

$$s_j \equiv (\Phi'_j, \Phi'_j) = \sum_{m \in \mathcal{S}_j} p_m^2. \quad (2.6)$$

We show below, that

$$\sum_{j=1}^{\infty} s_j = 1, \quad (2.7)$$

that allows us to understand s_j as a portion of the cross-section area, occupied by the j -zone. Then, the first of Eqs. (0.10) gives the definition of S_j , the area of j -zone, that is consistent with the requirement $\sum_{j=1}^{\infty} S_j = S_{\perp}$.

To find R_j from Eq. (2.5) compute also

$$(\Phi''_j, \Phi''_j) = \frac{1}{R_j^2} \sum_{m \in \mathcal{S}_j} \mathcal{R}_m^2. \quad (2.8)$$

Then

$$R_j^2 = s_j^{-1} \sum_{m \in \mathcal{S}_j} \mathcal{R}_m^2. \quad (2.9)$$

2. Orthogonality and normalization conditions

By construction (2.4–2.5) the *PM*-basis is orthogonal in the sense:

$$(\Phi_j, \Phi_{j'}) = 2s_j \Delta_{jj'} , \quad (2.10a)$$

$$(\Phi_j^*, \Phi_{j'}) = 0 . \quad (2.10b)$$

The idea behind the choice (2.4) is that the functions Φ_j' and Φ_j'' form the *exact* expansions of the uniform profile of unit height (Φ_j') and of the linear profile (Φ_j''):

$$\sum_j \Phi_j'(\rho) = \hat{\mathbf{x}} , \quad (2.11a)$$

$$\sum_j R_j \Phi_j''(\rho) = -\mathcal{R} . \quad (2.11b)$$

These relations can be easily proven by projection of both sides of Eq. (2.11) onto the Laplace basis ϕ_m^\pm , using (2.3) and the definition of the *PM*-functions $\Phi_j(\rho)$, Eq. (2.4).

Let us show that Eq. (2.7) follows from the obvious constrain $(\hat{\mathbf{x}}, \hat{\mathbf{x}}) = 1$, after substitution $\hat{\mathbf{x}}$ from Eq. (2.11a). Using also the orthogonality conditions (2.10) one gets

$$\begin{aligned} 1 &= (\hat{\mathbf{x}}, \hat{\mathbf{x}}) = \sum_{j,j'=1}^{\infty} (\Phi_j', \Phi_{j'}') \\ &= \frac{1}{4} \sum_{j,j'=1}^{\infty} (\Phi_j + \Phi_j^*, \Phi_{j'} + \Phi_{j'}^*) = \sum_{j=1}^{\infty} s_j . \end{aligned}$$

We proved that all s_j add up to unity according to Eq. (2.7).

3. *PM*-expansions

Introduce the *PM*-projector

$$\begin{aligned} \hat{\mathbf{P}}_{PM} \{ \mathbf{f}(\rho) \} &= 2 \operatorname{Re} \sum_j \frac{(\Phi_j, \mathbf{f})}{(\Phi_j, \Phi_j)} \Phi_j(\rho) \\ &= \operatorname{Re} \sum_j s_j^{-1} (\Phi_j, \mathbf{f}) \Phi_j(\rho) , \end{aligned} \quad (2.12)$$

and define the *PM*-velocity $\mathbf{V}_{PM}(\rho, t)$ as the projection of the full field $\mathbf{V}(\rho, t)$ on the *PM*-basis:

$$\mathbf{V}_{PM}(\rho) = \hat{\mathbf{P}}_{PM} \{ \mathbf{V}(\rho) \} . \quad (2.13)$$

Using the normalization (2.10) one gets

$$\mathbf{V}_{PM}(\rho, t) \equiv \operatorname{Re} \left\{ \sum_{j=1}^{\infty} V_j(t) \Phi_j(\rho) \right\} , \quad (2.14a)$$

$$s_j V_j(t) \equiv (\Phi_j, \mathbf{V}) = (\Phi_j, \mathbf{V}_{PM}) . \quad (2.14b)$$

The expansion coefficients $V_j(t)$ can be understood as *PM*velocities in the zone representation. They play the

major role in our theory and will be called hereafter “the *PM*-velocities” or “zone velocities”.

Substituting $\hat{\mathbf{x}}$ and \mathcal{R} from Eqs. (2.11) into the definitions (2.1) of \mathcal{P} and \mathcal{M} , one gets with the help of Eqs. (2.14) the *PM*-expansion of the linear in \mathbf{V} integrals of motion:

$$\mathcal{P} = \sum_{j=1}^{\infty} (\Phi_j', \mathbf{V}) = \sum_j s_j V_j'(t) , \quad (2.15a)$$

$$\mathcal{M} = \sum_{j=1}^{\infty} R_j (\Phi_j'', \mathbf{V}) = \sum_j s_j (R_j V_j''(t)) . \quad (2.15b)$$

This is a proof of the statement that only *PM* part of the full velocity $\mathbf{V}(\rho, t)$, Eq. (2.14), contribute to the mechanical momenta. The turbulent part $\mathbf{V}_T(\rho)$ *does not contribute* to the linear integrals of motion and will be considered as a part of the “turbulent ensemble”, described by the shell variables $u_{nj}(t)$.

The energy density associated with the *PM*-velocity is as follows:

$$\mathcal{E}_{PM}(t) \equiv \int_{S_{\perp}} \frac{|\mathbf{V}_{PM}(\rho, t)|^2}{2} \frac{d\rho}{S_{\perp}} = \sum_{j=1}^{\infty} s_j \frac{|V_j(t)|^2}{2} . \quad (2.16)$$

4. *PM*-basis for the channel and pipe flows

The particular form of the *PM*-functions is geometry dependent. To give a feeling how these functions may look like, we discuss here two important cases, the channel and the pipe flows. These two examples will serve us in the rest of the paper. Some properties of these specific bases are however more general and will be used in the derivation and analysis of the momentum equation for $V_j(t)$.

In the planar geometry, Fig. 1, $\rho \Rightarrow y$ and the functions ϕ_m^\pm in Eq. (2.4) are given by

$$\phi_m^+(y) = \hat{\mathbf{x}} \phi_{2m-1}(y) , \quad (2.17a)$$

$$\phi_m^-(y) = \hat{\mathbf{z}} \phi_{2m}(y) ,$$

$$\phi_m(y) = \sqrt{2} \sin(k_m y) , \quad k_m = \pi m / (2H) ,$$

$$p_m = \frac{2\sqrt{2}}{\pi (2m-1)} \simeq 0.9 / (2m-1) . \quad (2.17b)$$

For the pipe geometry,

$$\phi_m^+(\rho) = \hat{\mathbf{x}} \phi_m(\rho) , \quad \phi_m^-(\rho) = \hat{\mathbf{e}} \phi_m(\rho) , \quad (2.18a)$$

$$\phi_m(\rho) = J_0(k_m \rho) / J_1(k_m R) , \quad (2.18b)$$

$$J_0(k_m R) = 0 , \quad p_m = 2 / (k_m R) , \quad (2.18c)$$

where $\hat{\mathbf{e}}$ is the polar-angle unit vector ($\hat{\mathbf{e}} \perp \hat{\mathbf{x}}$, $\hat{\mathbf{e}} \perp \hat{\rho}$), $J_0(\xi)$ and $J_1(\xi)$ are the Bessel functions of the 0-th and 1-st order, and R is the radius of the pipe. First of Eq. (2.18c) defines $k_m = \xi_m / R$ via zeros of the Bessel functions ξ_m : $J_0(\xi_m) = 0$.

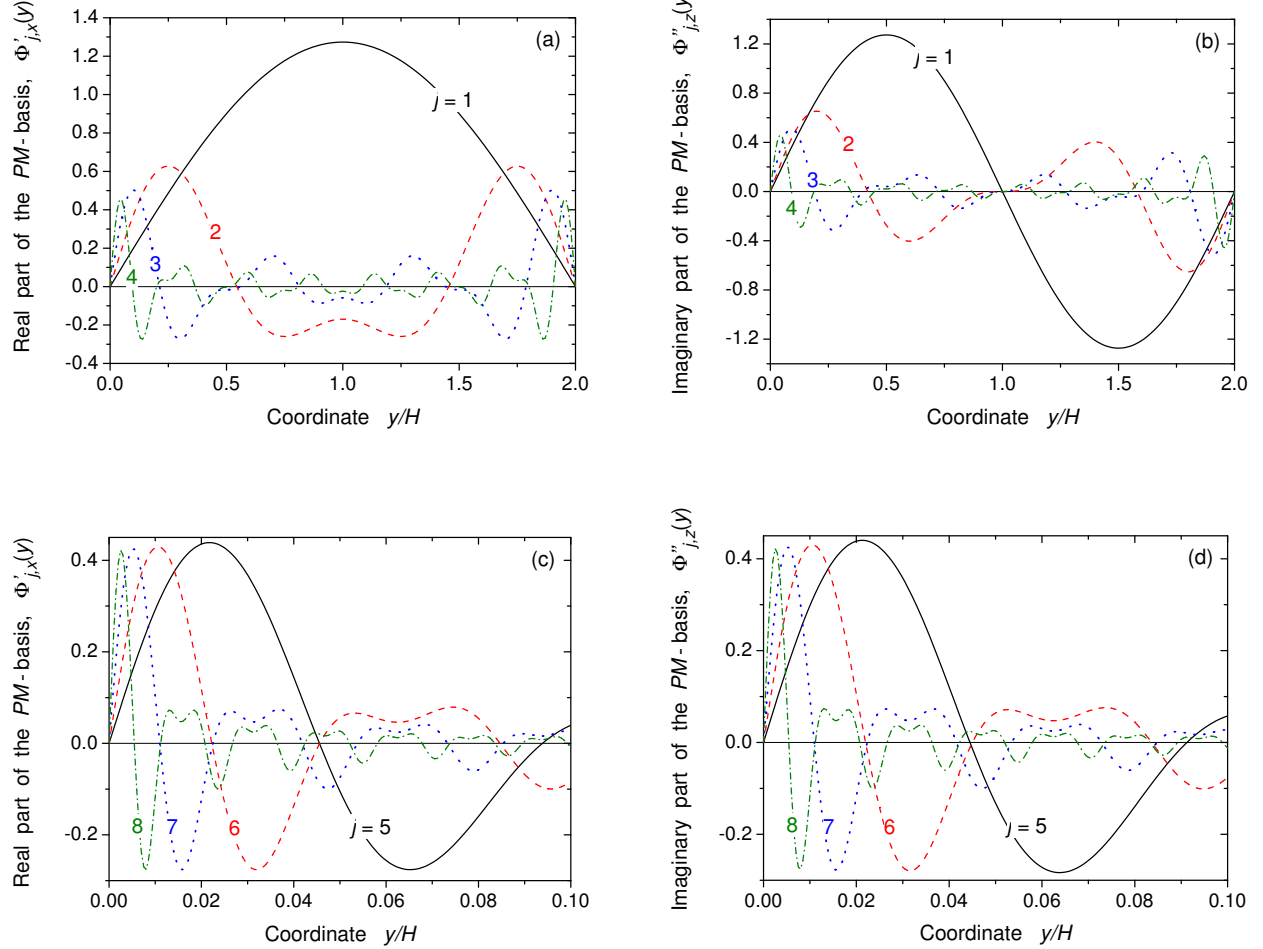


FIG. 3: First functions $\Phi_j(\xi H)$ describing the mean flow with non-zero mechanical momenta in the channel of the width $2H$. In the whole channel $0 < \xi < 2$. Panels *a* and *b*: the *PM*-functions $\Phi'_{j,x}(\xi H)$ (Panel *a*) and $\Phi''_{j,z}(\xi H)$ (Panel *b*) with $j = 1, 2, 3, 4$ for the whole channel. Panels *c* and *d*: the *PM*-functions with $j = 5, 6, 7, 8$ in the near-wall region. Panel *c*: $\Phi'_{j,x}(\xi H)$. Panel *d*: $\Phi''_{j,z}(\xi H)$.

In Fig. 3 we plot $\Phi'_{j,x}(y)$ and $\Phi''_{j,z}(y)$ for the channel as it follows from Eq. (2.4) with Eq. (2.17). The functions $\Phi'_{j,x}(y)$ are symmetric with respect to the centerline of the channel $y = H$, whereas $\Phi''_{j,z}(y)$ are antisymmetric. For large j , $\Phi'_{j,x}(y)$ and $\Phi''_{j,z}(y)$ coincide in the lower half of the channel $y < H$ and have an opposite sign for $y > H$. As it is clear from Panels *c* and *d*, in the near-wall ($y \ll H$) region $\Phi'_{j,x}(y)$ and $\Phi''_{j,z}(y)$ almost coincide already for $j = 5$.

For the channel flow one can find an explicit asymptotic expression for $\Phi'_{j,x}(y)$ and $\Phi''_{j,z}(y)$ in the limit $j \rightarrow \infty$ (actually, $j > 4$). For $y < H$:

$$\Phi'_{j,x}(y) \simeq \Phi''_{j,z}(y) \simeq \Phi_{\text{un}}(2^j \pi^2 y / 2H), \quad (2.19)$$

$$\Phi_{\text{un}}(\xi) \equiv \frac{2}{\pi} \left[\text{Si} \left(\frac{2\xi}{\pi} \right) - \text{Si} \left(\frac{\xi}{\pi} \right) \right], \quad (2.20)$$

where $\text{Si}(x)$ is the sine integral function.

It is expected, that the asymptotic form of basic functions, Φ_{un} , is the same for any flow geometry, if one express them as functions of the distance from the wall. For example, in the pipe one obtains (2.19), where y is the distance from the wall, $y = R - \rho$, and H is the radius of the pipe, $H = R$. In Fig. 4 we show the collapse of the re-scaled functions $\Phi_j(2H\xi/\pi^2 2^j)$ for $j = 5, \dots, 8$ with the universal function $\Phi_{\text{un}}(\xi)$ for the channel (Panel *a*) and pipe, $H = R$ flows.

5. Geometry of the j -zones in the channel and pipe flows

a. Characteristic length of a flow. The cross-section of the flow can be characterized by two global parameters, the cross-section area, S_{\perp} , and the length of its perimeter P_{\perp} . One can organize from these two objects many combinations with the dimensions of the length,

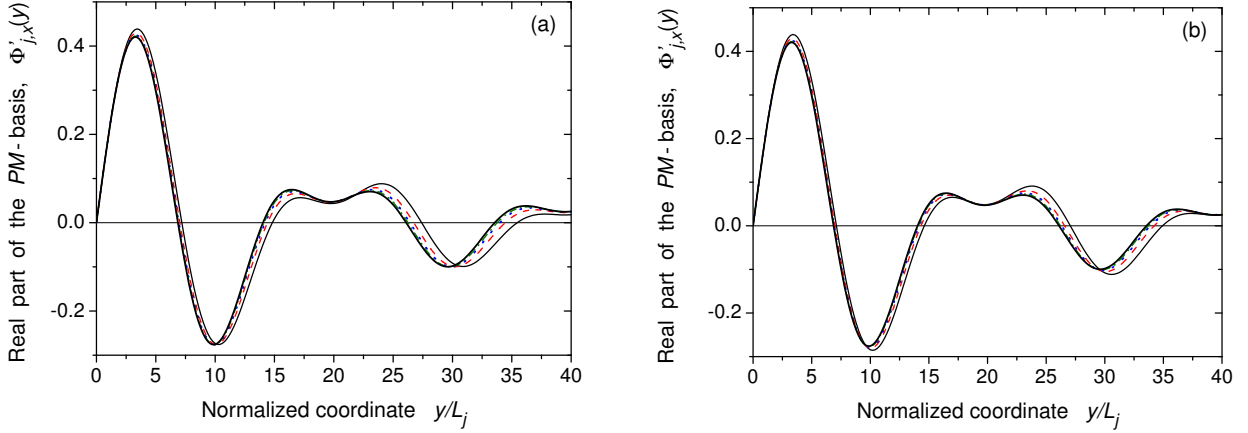


FIG. 4: Asymptotic universality of the *PM*-basis functions. Panel *a*: Collapse of the re-scaled real part of the basis functions $\Phi_j(2H\xi/\pi^2 2^j)$ for $n = 5 \dots 8$ with the universal asymptotic function $\Phi_{\text{un}}(\xi)$ for the channel flow. The lines (from right to left) correspond to those in Fig. 3c. The left-most solid line denote $\Phi_{\text{un}}(\xi)$. Panel *b*: the same for the pipe flow, $H = R$.

$L(\beta) \equiv P_\perp(S_\perp/P_\perp^2)^\beta$, with arbitrary β . For discussion of a turbulent flows under the external pressure gradient, the particular choice, $\beta = 1$,

$$L \equiv L(1) = S_\perp/P_\perp, \quad (2.21)$$

is physically important. The reason is that the total external accelerating force, applied on the unite length of the fluid (in the streamwise direction), is proportional to S_\perp :

$$F_{\text{ac}} = \nabla p S_\perp,$$

while the total friction force is proportional to P_\perp (under simplifying assumption of homogeneity along the perimeter):

$$F_{\text{fric}} = \nu_0 P_\perp \frac{dV_x(y)}{dy} \Big|_{y=0}.$$

The stationarity condition, $F_{\text{ac}} = F_{\text{fric}}$, allows one to relate $[dV_x(y)/dy]_{y=0}$ to the characteristic length, L defined by Eq. (2.21):

$$\frac{dV_x(y)}{dy} \Big|_{y=0} = \frac{\nabla p}{\nu_0 L}.$$

In terms of the friction velocity, U_τ , Eq. (0.7), and the friction Reynolds number, \mathcal{Re} , Eq. (0.8), this gives the famous constraint for the wall bounded flows:

$$\frac{dV_x(y)}{dy} \Big|_{y=0} = \mathcal{Re} \frac{U_\tau}{L}. \quad (2.22)$$

In all mentioned global relationships the characteristic length L plays an important role.

Notice that for the channel of the width $2H$ the length L is the distance from the centerline to a wall, $L = H$. For the pipe of the radius R the length $L = R/2$, which is twice smaller than the distance from the center to the wall.

TABLE I: Parameters of the *PM*-basis for the planar and pipe geometries.

j	Planar				Pipe			
	s_j	$s_j 2^j$	R_j/H	ν_j/ν_0	s_j	$s_j 2^j$	R_j/R	ν_j/ν_0
1	0.811	1.62	0.50	6.48	0.692	1.38	0.51	2.77
2	0.122	0.49	0.77	1.96	0.185	0.74	1.03	1.48
3	0.038	0.30	0.90	1.22	0.068	0.54	1.00	1.09
4	0.015	0.25	0.95	0.99	0.029	0.47	1.00	0.94
5	0.007	0.22	0.98	0.89	0.014	0.44	1.00	0.87
6	0.003	0.21	0.99	0.85	0.007	0.42	1.00	0.84
7	0.002	0.21	0.99	0.83	0.003	0.41	1.00	0.82
8	0.001	0.21	1.00	0.82	0.002	0.41	1.00	0.82
∞	—	$2/\pi^2$	1	$8/\pi^2$	—	$4/\pi^2$	1	$8/\pi^2$

b. Zones in the channel and pipe. In Tab. I we present parameters s_j for the channel and pipe geometries, that are given by Eq. (2.6) via p_m . The parameters p_m are taken from Eq. (2.17b) for the channel, and from Eq. (2.18c) for pipe geometry.

Using s_j and L we introduce the *characteristic width of the j -zone*:

$$L_j \equiv s_j L. \quad (2.23)$$

The idea behind this definition is that for the narrow near-wall zones L_j is exactly their geometrical width, Δ_j , i.e. the distance between the j -zone boundaries.

Assuming that Δ_j is much smaller than the local curvature of the boundary, we evaluate the area of very narrow j -zone as $S_j = \Delta_j P_\perp$. On the other hand, this area is $s_j S_\perp$. Therefore,

$$\Delta_j = s_j S_\perp / P_\perp = s_j L = L_j, \quad \text{for } j \gg 1.$$

TABLE II: Geometrical and characteristic widths Δ_j and L_j of j -zone in the pipe geometry

j	1	2	3	4	5	6
Δ_j/R	0.83	0.105	0.0356	0.0148	0.0071	0.0035
L_j/R	0.35	0.093	0.0340	0.0145	0.0070	0.0035

Obviously, for the planar geometry, $\Delta_j = L_j$ for any j . To find the value of j , at which the zones become flat, consider the pipe geometry with $\Delta_j = r_j - r_{j-1}$, where r_j is the radius of the circle, occupied by the first j -zones:

$$r_j = R \left[\sum_{i=1}^j s_i \right]^{1/2}, \quad \text{pipe}. \quad (2.24)$$

Table II compares Δ_j/R , given by this equation with $L_j/R = s_j/2$. Clearly, for $j > 3$ these two parameters practically coincide.

6. Interpretation of the PM-velocities

The PM -expansions of the linear profiles (2.11) gives a simple interpretation of the velocities $V'_j(t)$ and $V''_j(t)$ as the $\hat{\mathbf{x}}$ - and $\hat{\mathbf{e}}$ -projections of $\mathbf{V}_{PM}(\rho, t)$ at some position within the j -zone, ρ_j :

$$V'_j(t) \Leftrightarrow V_x(\rho_j, t), \quad V_x(\rho, t) \equiv \hat{\mathbf{x}} \cdot \mathbf{V}_{PM}(\rho, t), \quad (2.25a)$$

$$V''_j(t) \Leftrightarrow V_e(\rho_j, t), \quad V_e(\rho, t) \equiv \hat{\mathbf{e}} \cdot \mathbf{V}_{PM}(\rho, t), \quad (2.25b)$$

$$\hat{\mathbf{e}} \equiv \hat{\mathbf{x}} \times \rho / \rho. \quad (2.25c)$$

This point will be illustrated below in Fig. 14 by direct comparison of V_j and $V(\rho)$ in appropriate coordinates.

C. Simple momentum equation for V_j

Consider the NSE for $\mathbf{V}_{PM}(\rho, t)$ in the form:

$$\begin{aligned} \frac{\partial \mathbf{V}_{PM}(\rho, t)}{\partial t} &= -\nu_0 \Delta \mathbf{V}_{PM} + \nabla p \hat{\mathbf{x}} \\ &\quad - (\mathbf{V}_{PM} \cdot \nabla) \mathbf{V}_{PM} - \overline{(\mathbf{u} \cdot \nabla) \mathbf{u}}. \end{aligned} \quad (2.26)$$

Here ν_0 is the kinematic viscosity, $\nabla p = -dp/dx > 0$ is the pressure gradient in the streamwise direction $\hat{\mathbf{x}}$. The nonlinear term $(\mathbf{V}_{PM} \cdot \nabla) \mathbf{V}_{PM}$ describes the self-nonlinearity in the PM -subsystem and the last term, $(\mathbf{u} \cdot \nabla) \mathbf{u}$, is responsible for the effect of the Reynolds stress on the PM -velocity. Here $\overline{\dots}$ is the ensemble averaging in the sense of Eq. (1.10). The nonlinear cross term, $\propto V u$ (which has zero mean) is neglected.

The goal is to get the equation of motion for the complex PM -velocities $V_j(t)$:

$$\begin{aligned} \frac{dV_j}{dt} &= (\text{damping})_j + (\text{pressure})_j \\ &\quad + (\text{self-interaction})_j + (\text{Reynolds-stress})_j, \end{aligned} \quad (2.27)$$

by projecting NSE (2.26) on the PM -basis, using Eqs. (2.10) and (2.14b) in the form:

$$V_j(t) = 2(\Phi_j, \mathbf{V}_{PM}) / (\Phi_j, \Phi_j). \quad (2.28)$$

1. The damping term

Projecting the NSE (2.26) on the real and imaginary parts of the PM -basis Eq. (2.4), and accounting only for the viscous term, $\propto \nu_0$, one gets

$$\frac{dV'_j}{dt} = -\Gamma'_j V'_j, \quad \frac{dV''_j}{dt} = -\Gamma''_j V'_j,$$

with, generally speaking, different Γ'_j and Γ''_j :

$$\Gamma'_j = -\nu_0 \frac{(\Phi'_j, \Delta \Phi'_j)}{(\Phi'_j, \Phi'_j)}, \quad \Gamma''_j = -\nu_0 \frac{(\Phi''_j, \Delta \Phi''_j)}{(\Phi''_j, \Phi''_j)}. \quad (2.29)$$

However, in the pipe flow they are equal, $\Gamma'_j = \Gamma''_j$, since the functions ϕ_m^+ and ϕ_m^- are the same, see Eq. (2.18). In the channel flow these functions, Eq. (2.17), are different and hence $\Gamma'_j \neq \Gamma''_j$. Nevertheless, for large j , the basis functions $\Phi'_j \rightarrow \Phi''_j$ and $\Gamma'_j \rightarrow \Gamma''_j$. Therefore it would be a reasonable simplification to neglect the (possible) difference between Γ'_j and Γ''_j and to write in Eq. (2.27):

$$(\text{damping})_j = -\Gamma_j V_j, \quad (2.30)$$

with the same damping term Γ_j , which is in between Γ'_j and Γ''_j . For example, in the channel flow, V'_j is responsible for the mean velocity profile $V_x(y)$ and thus “more important” than V''_j . In that case we will take $\Gamma_j = \Gamma'_j$. In the planar Couette flow, the mean velocity profile is given by $V_z(y)$, which is connected to V''_j , and thus one better take $\Gamma_j = \Gamma''_j$.

It is customary to represent the damping term via an effective viscosity, ν_j , and an effective wave-vector, κ_j , defined via the characteristic width of the j -zone L_j :

$$\Gamma_j = \nu_j \kappa_j^2, \quad \nu_j \sim \nu_0, \quad (2.31)$$

$$\kappa_j \equiv \frac{1}{2L_j}, \quad L_j \equiv s_j L. \quad (2.32)$$

Parameters L and L_j were defined and discussed in Sec. II B 5 b. The values of s_j and ν_j for the channel and pipe flows are presented in Tab. I.

Notice, that the damping term in Eq. (2.30) is diagonal in j . This is a consequence of our definition of the PM -functions Φ_j , Eq. (2.4): the functions with different j originate from different, and thus *orthogonal* eigenfunctions of the Laplace operator.

2. The pressure term

The equations (2.26) and (2.28) dictate:

$$(\text{pressure})_j = 2\nabla p (\Phi_j, \hat{\mathbf{x}}) / (\Phi_j, \Phi_j).$$

Substituting $\hat{\mathbf{x}}$ from Eq. (2.11a) into above expression, one gets for any flow geometry the same simple expression:

$$(\text{pressure})_j = \nabla p . \quad (2.33)$$

This means, that the uniform in ρ pressure gradient equally acts on all components $V'_j(t)$. This remarkable result could be also obtained from the interpretation of V_j , Sec. II B 6. Indeed, if we leave in the RHS of Eq. (2.26) only the pressure term, we get the ρ -independent $V_x(\rho, t) = \nabla p t$, i.e. a homogeneous velocity profile. This means that $V'_j(t)$ is independent of j .

3. The self-interaction term

In various simple flows the self-interaction term in Eq. (2.26) is identically equal to zero due to geometrical constraint. It is so for the channel and the planar Couette flows, where

$$(\mathbf{V} \cdot \nabla) \mathbf{V} \Rightarrow \left(V_x \frac{\partial}{\partial x} + V_z \frac{\partial}{\partial z} \right) \mathbf{V}(y) \equiv 0 .$$

Here we skipped for the brevity the subscript “_{PM}”. The same is true for the pipe geometry, where

$$(\mathbf{V} \cdot \nabla) \mathbf{V} \Rightarrow \left(V_x \frac{\partial}{\partial x} + \frac{V_\phi}{\rho} \frac{\partial}{\partial \phi} \right) \mathbf{V}(\rho) \equiv 0 .$$

In the present paper we consider only flows with zero self-interaction:

$$(\text{self-interaction})_j = 0 . \quad (2.34)$$

4. Effect of the Reynolds stress

In the *PM*-representation the Reynolds-stress term in Eq. (2.27) should be quadratic function of the turbulent velocities u_{nj} and should scale as $\kappa_j \equiv 1/(2L_j) \propto 2^j$. This term describes two physical processes, namely, (i) the exchange of the linear and angular momenta between different zones and, (ii) together with its counterpart w_j in the equation for u_{nj} , the energy exchange between V_{j-1} and u_{nj} -subsystems.

In the spirit of the shell models of turbulence, we consider here the form the Reynolds-stress term that accounts for the momenta exchange only between nearest j -zones (j and $j \pm 1$) and preserves the relevant integrals of motions, the energy and the momenta. Notice, that in the turbulent channel and pipe flows with $\langle \mathcal{M} \rangle = 0$, the conservation of \mathcal{P} is much more important than the conservation of \mathcal{M} . Therefore we can simplify the possible structure of the inter-system interaction terms, W_j and w_j by using instead of Eq. (2.15b) for \mathcal{M} its simplified version, in which all R_j are assumed to be the same, $R_j \rightarrow R_\infty = \text{const}$, and thus can be omitted:

$$\tilde{\mathcal{M}} = \sum_j s_j V_j'' \Rightarrow \text{Quasi-angular momentum.} \quad (2.35)$$

It is easily justified by noting that for $j > 3$ the j -zone contributions to \mathcal{M} and $\tilde{\mathcal{M}}$ are almost the same, see Table I for R_j . In the following we will drop the tilde in $\tilde{\mathcal{M}}$, and write quasi-angular momentum simply as \mathcal{M} . Having in mind the conservation of the “complex momentum”:

$$\mathcal{L} \equiv \mathcal{P} + i \mathcal{M} = \sum_j s_j V_j ,$$

we suggest the following form of the Reynolds-stress term, W_j :

$$(\text{Reynolds-stress})_j \equiv W_j = \frac{1}{s_j} (\mathfrak{p}_{j-1} - \mathfrak{p}_j) , \quad (2.36)$$

where \mathfrak{p}_j is the momentum flux from the j - to the $(j+1)$ -zone. Indeed, this form provides the conservation of \mathcal{L} in the inviscid, unforced limit:

$$\frac{d\mathcal{L}}{dt} = \sum_j s_j W_j = \sum_j (\mathfrak{p}_{j-1} - \mathfrak{p}_j) = 0 .$$

For the momentum flux \mathfrak{p}_j we also select the simplest form, assuming that only the near-wall turbulent eddies of the same scale $u_{jj} \equiv u_j$ (i.e. u_{nj} with $n = j$) give a nonzero momentum transfer:

$$\mathfrak{p}_j = \frac{d}{2L} u_j^2 . \quad (2.37)$$

Here the dimensionless parameter d characterize the strength of the interactions.

The equations (2.36) and (2.37) give us the following simple expression for W_j :

$$W_j = d \kappa_j (u_{j-1}^2 - u_j^2) . \quad (2.38)$$

The production term w_j , describing the energy pumping into j -zone of the turbulent subsystem, Eq. (1.12), is then uniquely determined by the requirement of the conservation of the total energy of the system:

$$w_j = \frac{d}{2\sigma_j L} (V_j - V_{j+1}) u_j^* . \quad (2.39)$$

5. Resulting momentum equation

Collecting Eqs. (2.27), (2.30) – (2.34) and (2.36) one finally gets:

$$\frac{dV_j(t)}{dt} = -\nu_j \kappa_j^2 V_n + \nabla p + W_j , \quad (2.40)$$

where ν_j is the effective viscosity, given for the channel and the pipe flows in Table I, κ_j is given by Eq. (2.32) and W_j – by Eq. (2.38). This equation together with Eq. (1.12) will be analytically and numerically analyzed in the following Secs. III and IV.

III. CONSERVATION LAWS AND SYMMETRIES IN THE MZS-MODEL

A. Resulting dimensionless MZS-equations

For the convenience of the reader we present here the full set of the MZS-equations which will be the subject of analytical and numerically studies. As the first step, we non-dimensionalize the MZS-equations, expressing time t and velocities V_j , u_{nj} in the units τ and U_τ :

$$\tilde{t} \equiv \frac{t}{\tau}, \quad (3.1a)$$

$$\tilde{V}_j(\tilde{t}) \equiv \frac{V_j(\tau \tilde{t})}{U_\tau}, \quad (3.1b)$$

$$\tilde{u}_{nj}(\tilde{t}) \equiv \frac{u_{nj}(\tau \tilde{t})}{U_\tau}, \quad (3.1c)$$

$$\nabla \tilde{p} = 1, \quad (3.1d)$$

where time, τ , and velocity, U_τ , are constructed from the “outer” characteristics of the flow, ∇p and L :

$$\tau \equiv \sqrt{L/\nabla p}, \quad U_\tau \equiv \sqrt{\nabla p L}. \quad (3.2)$$

In the rest of the paper we omit the tildes in the dimensionless variables. The dimensionless MZS-equations take on the form:

$$\frac{dV_j}{dt} = -\Gamma_j V_j + \nabla p_j + W_j, \quad \nabla p_j = \nabla p = 1 \quad (3.3a)$$

$$\begin{aligned} \frac{du_{nj}}{dt} &= -\gamma_n u_{nj} + \mathcal{N}_{nj} + \Delta_{nj} w_j, \\ j &= 1, 2, \dots, \infty, \quad n = j, j+1, \dots, \infty. \end{aligned} \quad (3.3b)$$

Here the shell variables u_{nj} are the velocities of statistically identical (nj) -eddies of characteristic scale s_n that belong to j -zone of width s_j . Clearly, in Eqs. (3.3b) $n \geq j$. The *PM*-variables $V_j(t)$ describe the velocities of coherent near-wall structures in the j -zone. In our notations the near wall turbulent (nj) -eddies have $n = j$. These eddies occupy also all j -zones with $j \geq n$. Therefore in our approach

$$u_{nj} = u_{nn} \equiv u_n, \quad \text{for} \quad j \geq n.$$

The terms in the RHS of the dimensionless MZS-equations (3.3) are as follows:

$$\Gamma_j = \frac{G_j}{\mathcal{R}e} \kappa_j^2, \quad \gamma_n = \frac{g_n}{\mathcal{R}e} \kappa_n^2, \quad \kappa_j \equiv \frac{1}{2s_j}, \quad (3.4a)$$

$$W_j = d\kappa_j (u_{j-1}^2 - u_j^2), \quad (3.4b)$$

$$w_j = \frac{d}{2\sigma_j} (V_j - V_{j+1}) u_j^*, \quad \sigma_j \equiv \sum_{j' \geq j} s_{j'}, \quad (3.4c)$$

$$\mathcal{N}_{nj} = N_{nj} + \Delta_{nj} \sum_{j' > j} \frac{s_{j'}}{\sigma_j} (N_{nj'} - N_{nj}), \quad (3.4d)$$

$$\begin{aligned} N_{nj} &= i(a \kappa_{n+1} u_{n+1,j}^* u_{n+2,j} \\ &+ b \kappa_n u_{n-1,j}^* u_{n+1,j} - c \kappa_{n-1} u_{n-2,j} u_{n-1,j}). \end{aligned} \quad (3.4e)$$

Here

$$a + b + c = 0, \quad \sum_{j \geq 1} s_j = 1.$$

The equations (3.4) contain only one physical parameter, the friction Reynolds number

$$\mathcal{R}e \equiv LU_\tau/\nu_0, \quad (3.5)$$

and a set of geometry-dependent, dimensionless factors G_j , g_n , and s_j . For the channel and pipe flows the factors $G_j = \nu_j/\nu_0$ and s_j are given in Table I. For simplicity in this paper we take $g_n = G_n$.

B. Conservation laws and fluxes

In the inviscid ($\Gamma_j = \gamma_n = 0$), unforced ($\nabla p_j = 0$) limit Eq. (3.3) conserves energy, \mathcal{E} , linear momentum, \mathcal{P} , and (quasi-) angular momentum, \mathcal{M} :

$$\mathcal{E} = \frac{1}{2} \sum_{j=1}^{\infty} s_j \left(|V_j|^2 + \sum_{n=1}^{\infty} |u_{nj}|^2 \right), \quad (3.6a)$$

$$\mathcal{P} = \sum_{j=1}^{\infty} s_j V'_j, \quad (3.6b)$$

$$\mathcal{M} = \sum_{j=1}^{\infty} s_j V''_j. \quad (3.6c)$$

In general case, with non-zero Γ_j , γ_j , and ∇p_j the direct calculation of $d\mathcal{E}/dt$, $d\mathcal{P}/dt$, and $d\mathcal{M}/dt$ with the help of Eq. (3.3) gives:

$$\frac{d\mathcal{E}}{dt} = \varepsilon^+ - \varepsilon^-, \quad (3.7a)$$

$$\frac{d\mathcal{P}}{dt} = \mathfrak{p}^+ - \mathfrak{p}^-, \quad (3.7b)$$

$$\frac{d\mathcal{M}}{dt} = \mathfrak{m}^+ - \mathfrak{m}^-. \quad (3.7c)$$

Here ε^+ , \mathfrak{p}^+ , and \mathfrak{m}^+ , are *total* influxes of respective integrals of motion, \mathcal{E} , \mathcal{P} , and \mathcal{M} , and ε^- , \mathfrak{p}^- , and \mathfrak{m}^- , are their *total* rates of dissipations. Similar to Eqs. (3.6) these objects can be represented as s_j -weighted sums, $\sum_j s_j (\dots)$, of the respective densities of *partial* influxes (ε_j^+ , \mathfrak{p}_j^+ , and \mathfrak{m}_j^+) and *partial* rates of dissipation in the j -zone:

$$\varepsilon^+ = \sum_{j=1}^{\infty} s_j \varepsilon_j^+, \quad \varepsilon_j^+ = \nabla p_j V'_j = V'_j, \quad (3.8a)$$

$$\mathfrak{p}^+ = \sum_{j=1}^{\infty} s_j \mathfrak{p}_j^+, \quad \mathfrak{p}_j^+ = \nabla p_j = 1, \quad (3.8b)$$

$$\mathfrak{m}^+ = \sum_{j=1}^{\infty} s_j \mathfrak{m}_j^+, \quad \mathfrak{m}_j^+ = 0, \quad (3.8c)$$

$$\varepsilon^- = \sum_{j=1}^{\infty} s_j \varepsilon_j^- , \quad \varepsilon_j^- = \Gamma_j |V_j|^2 + \sum_{n=1}^{\infty} \gamma_n |u_{nj}|^2 , \quad (3.9a)$$

$$\mathfrak{p}^- = \sum_{j=1}^{\infty} s_j \mathfrak{p}_j^- , \quad \mathfrak{p}_j^- = \Gamma_j V'_j , \quad (3.9b)$$

$$\mathfrak{m}^- = \sum_{j=1}^{\infty} s_j \mathfrak{m}_j^- , \quad \mathfrak{m}_j^- = \Gamma_j V''_j . \quad (3.9c)$$

The total influx of energy is exactly equal to the total linear momentum of the flow (due to our normalization, $\nabla p = 1$) and the total influx of the linear momentum equals to unity:

$$\varepsilon^+ = \nabla p \sum_{j=1}^{\infty} s_j V'_j = \nabla p \mathcal{P} = \mathcal{P} , \quad (3.10a)$$

$$\mathfrak{p}^+ = \nabla p \sum_{j=1}^{\infty} s_j = \nabla p = 1 . \quad (3.10b)$$

For the channel and pipe flows, the influx of the angular momentum, $\mathfrak{m}^+ = 0$. In the planar Couette flow, $\mathfrak{p}^+ = 0$ and $\mathfrak{m}^+ \neq 0$.

Notice, that the main part of the influx of the momentum is always flowing into the first few zones, where s_j have considerable values. For example, in the channel, $\approx 81\%$ of the total \mathfrak{p}^+ flows into the first zone (occupying $s_1 \approx 0.81$ part of the cross-section area, see Table I), 93% – into the first two zones and only about 1% to the fifth and all higher zones. As we show below, V'_j slightly decay with j , hence the influx of energy is even more confined to the first zones.

For very high Reynolds numbers the dissipation of the conserved quantities occurs at large j (or n), $\sim \log_2 \mathcal{Re}$. Therefore for $\log_2 \mathcal{Re} \gg 1$ there exist an inertial interval (generally speaking, different for the different quantities). Clearly, in the stationary case the influx of some conserved quantity have to be equal to its flux (in the shell space or via zones). For the energy, it is useful to analyze the energy flux in the shell space:

$$\varepsilon^+ = \varepsilon_n = \varepsilon^- = \mathcal{P} , \quad \varepsilon_n = \sum_{j=1}^{\infty} \varepsilon_{nj} , \quad (3.11)$$

where ε_{nj} is usual for the shell models (in the j -zone) expression for the flux of energy from n th to $(n+1)$ shell.

The flux of the linear momentum, \mathfrak{p}_j from j - to $(j+1)$ -zone is given by Eq. (2.37), which in the dimensionless form reads: $\mathfrak{p}_j = d u_j^2 / 2$. Therefore, in the stationary case, for j in the inertial interval

$$\mathfrak{p}_j = d u_j^2 / 2 = \mathfrak{p}^+ = \mathfrak{p}^- = 1 . \quad (3.12)$$

To get the expression for the value of \mathfrak{p}_j , valid for any j (not only in the inertial interval), we multiply Eq. (3.3a)

by the j -zone area, s_j , and sum up from 1 to j . This gives the useful equation

$$\mathfrak{p}_j = d u_j^2 / 2 = \sum_{i=1}^j s_i (1 - \Gamma_i V_i) , \quad \text{any } j , \quad (3.13)$$

that allows us to express the turbulent velocity $u_j = u_{jj}$, generating the turbulent energy cascade in the j -zone, via *PM*-velocities.

C. Galilean invariance of the model

The Galilean transformation to the reference system, moving with some velocity U_0 in the streamwise direction $\hat{\mathbf{x}}$, changes $\mathbf{V}(\rho, t) \Rightarrow_G \mathbf{V}(\rho, t) + \hat{\mathbf{x}} U_0$. According to Eqs. (2.11a) and (2.28) it leads to the transformation:

$$V_j(t) \Rightarrow_G V_j(t) + U_0 . \quad (3.14)$$

Clearly, the term w_j , Eq. (3.4c), describing the effect of the mean velocity on the turbulent subsystem, is Galilean invariant:

$$w_j = \frac{d}{2\sigma_j} (V_j - V_{j+1}) u_j^* \Rightarrow_G w_j . \quad (3.15)$$

In other words, the uniform velocity profile, $\mathbf{V}(\rho) = \hat{\mathbf{x}} \times \text{const}$, does not affect the statistics of turbulence. This important invariance of the MZS-equations guarantees that for $\mathcal{Re} \rightarrow \infty$ the mean velocity profile in the core of the flow becomes uniform and the statistics of turbulence becomes space homogeneous, as expected.

D. Asymptotic scale invariance and equations for the Turbulent Boundary Layer near flat plane

Consider MZS-Eqs. (3.3) at very large \mathcal{Re} in the near-wall region, $n, j > j_* \gg 1$, in which the dimensionless parameters in Eq. (3.4) can be already replaced by their asymptotic values:

$$G_j \Rightarrow G , \quad g_j \Rightarrow g , \quad (3.16)$$

$$s_j \Rightarrow 2^{-j} s , \quad \sigma_j \Rightarrow 2 s_j .$$

This is definitely so for the channel and pipe flows, say, for $j_* = 3$, see Tab. I. For large j the zone width is much smaller than the local curvature radius of the wall and the discussed situation corresponds to the case of *Turbulent Boundary Layer* (TBL) near the flat plane.

For $j \geq j_*$ the dimensionless flux of linear momentum from j - to $(j+1)$ -zone, \mathfrak{p}_j , is very close to 1 and much larger than the direct influx into j zone $s_j \mathfrak{p}_j^+ = s_j \ll 1$ from the external pressure gradient. Therefore in this regime one can neglect in the RHS of Eq. (3.3a) $\nabla p = 1$

with respect to W_j and simplify Eq. (3.3) to the scale-invariant form:

$$\frac{dV_j}{dt} = -\frac{G\kappa_j^2}{\mathcal{R}e}V_j + d\kappa_j(u_{j-1}^2 - u_j^2), \quad (3.17a)$$

$$\frac{du_{nj}}{dt} = -\frac{g\kappa_n^2}{\mathcal{R}e}u_{nj} + N_{nj} \quad (3.17b)$$

$$+ \frac{\Delta_{nj}}{2} \left[d\kappa_j(V_j - V_{j+1})u_j^* + \sum_{j'>j} 2^{j-j'}(N_{nj'} - N_{nj}) \right],$$

$$\kappa_j = 2^j \kappa, \quad \kappa = 1/2s, \quad n \geq j \geq j_*, \quad (3.17c)$$

$$\mathfrak{p}^+ = d u_{j*-2}^2/2 = d u_{j*-1}^2/2 = 1, \quad (3.17d)$$

where N_{nj} has already the scale invariant form Eq. (3.4e). The “TBL boundary condition” at $j = j_*$, (3.17d), provides the influx of energy and mechanical momentum into TBL, Eq. (3.17). In initial Eq. (3.3) this role is played by the external pressure gradient $\nabla p = 1$.

Equations (3.17) have additional [with respect to Eq. (3.3)] rescaling symmetry, namely, they remain unchanged under the transformation

$$\begin{aligned} V_j &\rightarrow \tilde{V}_j = V_{j+j_0}, \\ u_{nj} &\rightarrow \tilde{u}_{nj} = u_{n+j_0, j+j_0}, \\ t &\rightarrow \tilde{t} = t/2^{j_0}, \\ \mathcal{R}e &\rightarrow \tilde{\mathcal{R}e} = \mathcal{R}e/2^{j_0}, \end{aligned} \quad (3.18)$$

which corresponds (in the r -space) to the simultaneous rescaling of the outer scale L and the pressure gradient ∇p in a way that leaves the value of the wall shear stress unchanged, $\nabla p L = \text{const}$. This symmetry of the equations means that MZS-model describes the asymptotic universality of the near-wall turbulence for $\mathcal{R}e \rightarrow \infty$, and that the only relevant parameter in this regime is the total influx of the momentum, \mathfrak{p}^+ , which is fixed by the boundary conditions (3.17d).

In studies of the near-wall turbulence, it is customary to normalize the time and velocity units by the “inner” scales instead of the “outer” ones. Namely, we should use the *viscous length-scale* $\delta \equiv \nu_0/U_\tau = L/\mathcal{R}e$ instead of the outer scale L , and the corresponding timescale $\tau_\delta \equiv \delta/U_\tau = \tau/\mathcal{R}e$ instead of τ . As one can see, this rescaling corresponds to the choice $j_0 = \log_2 \mathcal{R}e$ in the transformation (3.18). In new units, the MZS-equations have the same form as (3.17) with $\mathcal{R}e = 1$:

$$\frac{dV_j}{dt} = -G\kappa_j^2 V_j + d\kappa_j(u_{j-1}^2 - u_j^2), \quad (3.19a)$$

$$\frac{du_{nj}}{dt} = -g\kappa_n^2 u_{nj} + N_{nj} \quad (3.19b)$$

$$+ \frac{\Delta_{nj}}{2} \left[d\kappa_j(V_j - V_{j+1})u_j^* + \sum_{j'>j} 2^{j-j'}(N_{nj'} - N_{nj}) \right],$$

where we omit tildes in the new variables. Equations (3.19) represent the *MZS model for TBL near flat plane*.

Unlike Eqs. (3.17), in Eqs. (3.19) the zone and scale indices, j and n , can be both positive and negative: thus,

V_0 corresponds to the velocity of the scale δ , V_{-1} – to the structures of the scale 2δ , and so on.

We can use general formulas (2.14a) to reconstruct the mean velocity profiles, $\mathbf{V}_{PM}(\boldsymbol{\rho})$. In this case the expression for $\mathbf{V}_{PM}(\boldsymbol{\rho})$ take on especially simple form, since all functions $\Phi_j(\boldsymbol{\rho})$ already have a scale-invariant form. Taking into account our rescaling to the “inner” units, we can write:

$$\mathbf{V}_{PM}(y) = \text{Re} \left[\sum_j V_j \Phi_{un}(2^j \pi^2 y/2\delta) \right], \quad (3.20)$$

where y is the distance to the wall, $\Phi_{un}(\xi)$ is given by (2.20) and $\mathbf{V}_{PM}(y)$ is measured in the units U_τ .

IV. SOLUTION OF THE MZS EQUATIONS

A. Laminar velocity profile and its instability

1. Comparison of the full and PM-laminar profiles

The simplest solution of MZS-equations (3.3), in which all $u_{nj} = 0$, corresponds to the laminar flow:

$$V_j = V_j^0 \equiv \frac{1}{\Gamma_j} = \frac{\mathcal{R}e}{G_j \kappa_j^2}. \quad (4.1)$$

Using Eq. (2.14a), one reconstructs the laminar profile of the *PM*-velocity

$$\mathbf{V}_{PM}^0(\boldsymbol{\rho}) = \sum_j V_j^0 \Phi_j'(\boldsymbol{\rho}) = \mathcal{R}e \sum_j \frac{\Phi_j'(\boldsymbol{\rho})}{G_j \kappa_j^2}. \quad (4.2)$$

The laminar profile of the full velocity, $\mathbf{V}^0(\boldsymbol{\rho})$, satisfy the linear NSE, which in the dimensionless form (3.1) reads

$$\Delta \mathbf{V}^0(\boldsymbol{\rho}) + \hat{\mathbf{x}} \mathcal{R}e = 0. \quad (4.3)$$

According to Eq. (2.13) the *PM*-velocity is understood as the *PM*-projection of the full velocity: $\hat{\mathbf{P}}_{PM}\{\mathbf{V}(\boldsymbol{\rho})\} = \mathbf{V}_{PM}(\boldsymbol{\rho})$. Therefore, we expect that the laminar *PM*-profile (4.2) satisfy the equation, similar to (4.3):

$$\hat{\mathbf{P}}_{PM}\{\Delta \mathbf{V}_{PM}^0(\boldsymbol{\rho})\} + \hat{\mathbf{x}} \mathcal{R}e = 0. \quad (4.4)$$

The proof of this equation is given in Appendix A.

In the case $\hat{\mathbf{P}}_{PM}\Delta = \Delta \hat{\mathbf{P}}_{PM}$ Eqs. (4.3) and (4.4) coincide, because $\hat{\mathbf{P}}_{PM} \mathbf{V}_{PM} = \mathbf{V}_{PM}$. If so, the functions $\mathbf{V}^0(\boldsymbol{\rho})$ and $\mathbf{V}_{PM}^0(\boldsymbol{\rho})$ have to coincide due to uniqueness of solutions of Eq. (4.3) with zero boundary condition. However, due to incompleteness of the *PM*-basis, $\hat{\mathbf{P}}_{PM}\Delta \neq \Delta \hat{\mathbf{P}}_{PM}$ and hence the profiles $\mathbf{V}^0(\boldsymbol{\rho})$ and $\mathbf{V}_{PM}^0(\boldsymbol{\rho})$ are expected to differ. In other words, Eq. (4.2) cannot reconstruct *exactly* the laminar profile $\mathbf{V}^0(\boldsymbol{\rho})$. This is the price to pay for the incompleteness the *PM*-basis. Nevertheless the *PM*-basis is “full enough” to allow the reconstruction of any “physically possible” mean velocity profile with

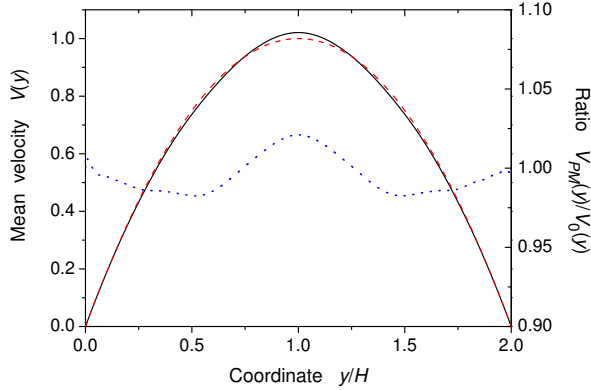


FIG. 5: Comparison of the exact (solid line) and *PM*- (dashed line) laminar profiles for the channel flow. The ratio of two profiles is shown by dotted line. Its values are marked on the right axis.

good accuracy. As a first demonstration of this fact we compare in Fig. 5 the exact and the *PM-laminar* profiles for channel flow, which differ only in few percents. This small loss of accuracy is insignificant with respect to a dramatic simplification of the calculation scheme for $\mathbf{V}(\rho, t)$: for large \mathcal{Re} the mean velocity field in *PM*-representation has $N \approx \ln \mathcal{Re}$ significant coefficients V_j , while in the corresponding complete cell basis one has to account for $\sim \mathcal{Re} \gg N$ functions.

2. Instability of the laminar flow at $\mathcal{Re} = \mathcal{Re}_{\text{cr}}$

The laminar solution (4.1) exists for all \mathcal{Re} . For large \mathcal{Re} , however, it becomes unstable with respect to excitation of turbulent near-wall eddies u_j . A simple analysis of the linearized Eq. (3.3b) (i.e. $\mathcal{N}_{nj} \Rightarrow 0$) shows that the instability condition of j -eddy reads:

$$\gamma_j < d(V_j - V_{j+1})/2\sigma_j . \quad (4.5)$$

Substituting here V_j from Eq. (4.1) one gets:

$$\frac{g_j \kappa_j^2}{\mathcal{Re}} < \frac{d}{2\sigma_j} \left(\frac{1}{G_j \kappa_j^2} - \frac{1}{G_{j+1} \kappa_{j+1}^2} \right) \mathcal{Re} ,$$

which can be rewritten as the condition for \mathcal{Re} :

$$\mathcal{Re} > \mathcal{Re}_j \equiv \kappa_j^{3/2} \sqrt{\frac{\sigma_j}{s_j} \frac{g_j G_j G_{j+1}}{d(G_{j+1} - G_j \kappa_j^2 / \kappa_{j+1}^2)}} . \quad (4.6)$$

It is clear that $\mathcal{Re}_j \propto \kappa_j^{3/2}$, therefore, usually the first unstable zone is the first one, $j = 1$.

We want to stress, that Eq. (4.6) gives a correct instability threshold only for the *first* unstable zone:

$$\mathcal{Re}_{\text{cr}} = \mathcal{Re}_1 = \kappa_1^{3/2} \sqrt{\frac{\sigma_1 g_1 G_1 G_2}{s_1 d(G_2 - G_1 \kappa_1^2 / \kappa_2^2)}} . \quad (4.7)$$

The excitation of turbulence in, say, first zone will lead to a significant momentum flux from the 1st to the 2nd zone. As a result, the mean velocity V_2 will increase, the 2nd zone velocity gradient $V_2 - V_3$ will increase too, and the instability condition for u_2 will be therefore satisfied for smaller Reynolds numbers than predicted by Eq. (4.6). We will show later, that the real instability threshold for j -th zone is proportional to $\mathcal{Re}_j \propto \kappa_j$, i.e. is much smaller than the “laminar” result (4.6).

B. Wall-bounded flows in the approximation of near-wall eddies ($a = b = c = 0$).

In the previous Sec. IV A we have found the laminar solution of the MZS-Eqs. (3.3) with $u_{nj} = 0$ and have shown that this solution becomes unstable at $\mathcal{Re} = \mathcal{Re}_{\text{cr}}$ with respect to excitation of the near wall velocity $u_1 \equiv u_{11}$. As the next step in this Section we analyze a much more general solution of Eqs. (3.3), that allows non-zero values of all near wall velocities, $u_{jj} \equiv u_j$. The jj -eddies can be excited by a direct interaction with the *PM*-velocities, V_j . To prohibit the turbulent cascades, leading to excitation of other nj -eddies (with $n > j$), one can neglect in Eq. (3.3b) the interaction term \mathcal{N}_{nj} (i.e. put $a = b = c = 0$). In this case the MZS-Eqs. (3.3) take on a simple form:

$$\frac{dV_j}{dt} = -\Gamma_j V_j + 1 + d\kappa_j (u_{j-1}^2 - u_j^2) , \quad (4.8a)$$

$$\frac{du_j}{dt} = -\gamma_j u_j + \frac{d}{2\sigma_j} (V_j - V_{j+1}) u_j^* . \quad (4.8b)$$

In the stationary regime ($d/dt = 0$) only the finite number $(m-1) \geq 0$ of turbulent velocities are non-zero, i.e., $u_j = 0$ for $j \geq m$. This number depends on \mathcal{Re} . As it follows from Eq. (4.8a), the *PM*-velocities V_j for $j > m$ coincide with the laminar ones:

$$V_j = V_j^0 = \Gamma_j^{-1} \sim 2^{-2j} \mathcal{Re} , \quad j > m = m(\mathcal{Re}) . \quad (4.9)$$

In the unstable region $j < m$, as it follows from Eq. (4.8b), the zone velocity difference, $\Delta V_j \equiv V_j - V_{j+1}$ coincide with its critical value, see Eq. (4.5):

$$\Delta V_j = \Delta V_j^{\text{cr}} = \frac{2\gamma_j \sigma_j}{d} = A_j / \mathcal{Re} , \quad (4.10)$$

$$A_j \equiv 2g_j \kappa_j^2 \sigma_j / d .$$

This allows one to find all V_j via the last velocity in the unstable region, V_m :

$$V_j = V_m + (B_m - B_j) / \mathcal{Re} , \quad (4.11)$$

$$B_j \equiv \sum_{i=1}^{j-1} A_i .$$

Multiplying Eq. (4.8a) by s_j and summing up from $j = 1$ to $j = m$, one finds the equation for V_m with the solution:

$$V_m = \frac{1 - \sigma_{m+1}}{C_m} \mathcal{R}e - \frac{D_m}{C_m \mathcal{R}e}, \quad (4.12a)$$

$$C_m \equiv \sum_{j=1}^m s_j G_j \kappa_j^2 \sim 2^m, \quad (4.12b)$$

$$D_m \equiv \sum_{j=1}^m s_j G_j \kappa_j^2 (B_m - B_j) \sim 2^{2m}. \quad (4.12c)$$

Note, that in spite of the large number of different parameters (A_m, \dots, D_m), all of them are provided with explicit expressions and can be easily evaluated.

Now one finds the total linear mechanical momentum \mathcal{P} (i.e. the total flux of the fluid) of the flow from its definition (3.6b) and Eqs. (4.9) and (4.12a) for V_j for $j \leq m$ and for $j > m$:

$$\begin{aligned} \mathcal{P} &= \sum_{j=1}^m s_j V_j + \sum_{j=m+1}^{\infty} s_j V_j^0 \quad (4.13a) \\ &= E_m \mathcal{R}e + F_m / \mathcal{R}e, \end{aligned}$$

$$E_m \equiv \frac{(1 - \sigma_{m+1})^2}{C_m} + \sum_{j=m+1}^{\infty} \frac{s_j}{G_j \kappa_j^2}, \quad (4.13b)$$

$$F_m \equiv \sum_{j=1}^m s_j (B_m - B_j) - \frac{(1 - \sigma_{m+1}) D_m}{C_m}.$$

So far we treated the last index m in the unstable zones as fixed. However, it depends on the Reynolds number $\mathcal{R}e$ and is defined from the condition

$$V_m - V_{m+1} < \Delta V_m^{\text{cr}} = \frac{A_m}{\mathcal{R}e},$$

which ensures that the turbulent velocity u_m will not be excited, $u_m = 0$. This condition can be written as

$$\mathcal{R}e^2 < \frac{A_m C_m + D_m}{1 - \sigma_{m+1} - C_m / (G_{m+1} \kappa_{m+1}^2)} \equiv \mathcal{R}e_m^2. \quad (4.14)$$

Actually, it will be exactly $(m - 1)$ excited turbulent velocities u_j , if

$$\mathcal{R}e_{m-1} < \mathcal{R}e < \mathcal{R}e_m. \quad (4.15)$$

The analysis shows that this condition selects the index m , for which the total momentum \mathcal{P} (4.13) has minimum value.

Let us analyze the dependence (4.13a) of the total momentum in the limit of extremely large Reynolds numbers, $\ln \mathcal{R}e \gg 1$, and, respectively, large critical zone numbers m . In this case we can use the scale-invariant limit for all parameters:

$$E_m = 2^{-m} \tilde{E}, \quad F_m = 2^m \tilde{F}, \quad \mathcal{R}e_m = 2^m \tilde{R}, \quad (4.16)$$

where \tilde{E} , \tilde{F} and \tilde{R} are some geometry-dependent constants. Now for Reynolds numbers inside the range (4.15)

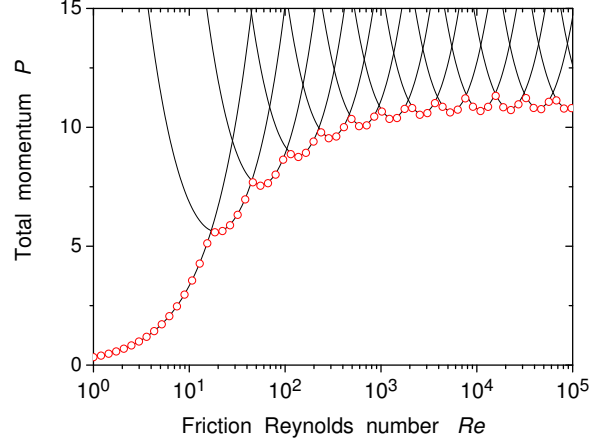


FIG. 6: Total momentum of the flow *vs.* the Reynolds number $\mathcal{R}e$. Circles denote numerical data for the channel flow, $d = 0.046$; solid lines - the analytical prediction (4.13) for different critical zone numbers m , $m = 1, 2, \dots$ (from left to right).

we can write in Eq. (4.13a) $x(\mathcal{R}e) = \mathcal{R}e / (2^m \tilde{R})$, where $1/2 < x(\mathcal{R}e) < 1$. Then \mathcal{P} for large enough $\mathcal{R}e$ [in the region of validity of the scale invariant limit (4.16)], is given by

$$\mathcal{P}(\mathcal{R}e) = x(\mathcal{R}e) \tilde{E} \tilde{R} + \frac{\tilde{F}}{x(\mathcal{R}e) \tilde{R}}. \quad (4.17)$$

Since $x(\mathcal{R}e)$ is bounded between 1/2 and 1, the flux (4.17) is bounded from above by one of the constants

$$\mathcal{P}(\mathcal{R}e) \leq \max \left\{ \frac{\tilde{E} \tilde{R}}{2} + \frac{2\tilde{F}}{\tilde{R}}, \tilde{E} \tilde{R} + \frac{\tilde{F}}{\tilde{R}} \right\}.$$

and does not grow infinitely for infinite Reynolds numbers. In other words, neglecting the dissipation of energy in turbulent cascades, one concludes that with the given cross-section area of the flow and pressure gradient, the total flux of the fluid reaches some limit in spite of the infinite decrease of the kinematic viscosity. The numerical and analytical calculations for the channel geometry, shown in Fig. 6, support this unexpected conclusion.

The reason for this strange behavior is that the stationary zone velocity differences, ΔV_j , in the unstable region $j < m$ are determined solely by the dissipation of turbulent eddies γ_j , Eq. (4.10), that go to zero as $\mathcal{R}e \rightarrow \infty$ (for finite j). Thus, in the limit $\mathcal{R}e \rightarrow \infty$, $\Delta V_j \rightarrow 0$ and $V_j \rightarrow \text{const}$. This conclusion is illustrated in Fig. 7. Clearly, for large $\mathcal{R}e$ first few velocities remain unchanged, and the only effect of increasing $\mathcal{R}e$ is the shift of the “dissipative cutoff” towards the smaller scales. However, the total momentum is determined mainly by the first few zones and thus remains the same.

This analysis shows importance of the turbulent cascade for the experimentally observed characteristics of

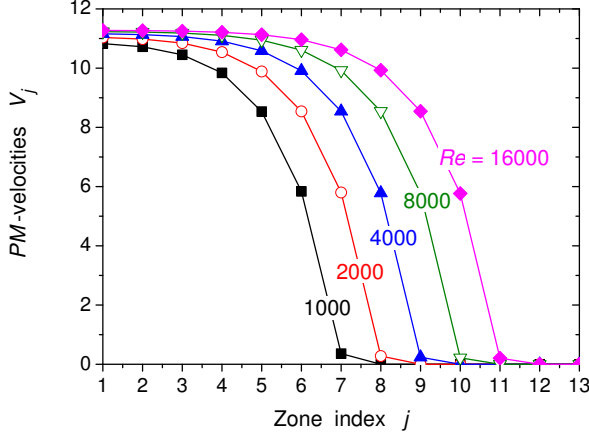


FIG. 7: Mean zone velocities V_j vs. the zone index j for different Reynolds numbers Re .

real flows, i.e. infinite increase of the total flux, logarithmic profiles, etc. The stationary condition $\Delta V_j = \Delta V_j^{\text{cr}}$ will hold even if one accounts for a turbulent cascade, which adds some *turbulent damping* γ_j^{T} for turbulent near-wall eddies instead of usual one γ_j . The turbulent damping *does not vanish in the limit* $Re \rightarrow \infty$. Thus, one obtains $\Delta V_j = \Delta V_j^{\text{cr}} \neq 0$, and the total momentum will infinitely increase, as it is shown in the following Sec. IV C.

C. Wall bounded flows in the “turbulent-viscosity” approximation

In this Section we show that even rough account for the turbulent cascade in the MZS-model already gives qualitatively correct analytical results.

1. MZS equations in the turbulent viscosity approximation

In the fully developed turbulent regime, the action of the interaction term \mathcal{N}_{nj} on the eddy u_{nj} can be approximately accounted for in the “turbulent viscosity” approximation in which the energy flux from the energy containing jj -eddies toward small scales in the j -zone is replaced by a nonlinear damping term, ensuring the same loss of their energy. Formally this can be done by replacing the nonlinear term \mathcal{N}_{jj} in the full MZS-Eqs. (3.19) by some effective turbulent damping term, γ_j^{T} :

$$\mathcal{N}_{jj} \Rightarrow -\gamma_j^{\text{T}} u_j, \quad \gamma_j^{\text{T}} = \alpha \kappa_j |u_j|, \quad (4.18a)$$

$$\alpha \approx (a - c). \quad (4.18b)$$

Here γ_j^{T} is chosen as the turnover frequency of jj -eddies, $\kappa_j |u_j|$ with some dimensionless prefactor α . This prefactor is evaluated in Eq. (4.18b) by equating the total rate

of energy dissipation in the model system with the effective turbulent damping (4.18a) and the energy flux toward small scales in the full shell model, see, e.g. Ref [3].

In the suggested *effective turbulent damping* approximation, the MZS-Eqs. (3.19) take the form

$$\frac{dV_j}{dt} = -\Gamma_j V_j + 1 + d\kappa_j (u_{j-1}^2 - u_j^2), \quad (4.19a)$$

$$\frac{du_j}{dt} = -(\gamma_j + \alpha\kappa_j |u_j|)u_j + \frac{d}{2\sigma_j} (V_j - V_{j+1}) u_j^*. \quad (4.19b)$$

These equations are different from the MZS-equations in the near-wall-eddy approximation, Eq. (4.8), by the only term $\propto \alpha$.

For large Re in the near wall region Eq. (4.19) have a more simple, scale-invariant form, in which all geometry dependent factors are taken in their small scale limit (3.16):

$$\frac{dV_j}{dt} = -\frac{G\kappa_j^2}{Re} V_j + 1 + d\kappa_j (u_{j-1}^2 - u_j^2), \quad (4.20a)$$

$$\frac{du_j}{dt} = -\left(\frac{g\kappa_j}{Re} + \alpha|u_j|\right)\kappa_j u_j + \frac{d\kappa_j}{2} (V_j - V_{j+1}) u_j^*, \quad (4.20b)$$

where $\kappa_j = 2^j/2s$.

2. Inertial interval solution

In this section we consider the stable stationary solution of Eq. (4.19). This solution is real.

For $\log_2 Re \gg 1$, in the inertial interval of scales, all needed information contained in Eq. (4.19a) may be obtained from Eq. (3.13) for the momentum flux, \mathfrak{p}_j , in which one can neglect the damping term $\propto 1/Re$. This gives

$$\mathfrak{p}_j = \frac{du_j^2}{2} = \sum_{j'=1}^j s_{j'} = 1 - \sigma_{j+1}, \quad (4.21)$$

where σ_j is defined by Eq. (3.4c). The substitution of u_j from Eq. (4.21) in Eq. (4.20b) gives an expression for V_{j+1} via V_j . This allows one to find V_j for any j outside the viscous region via some constant V_0 :

$$V_j = V_0 - \frac{\sqrt{2}\alpha}{d^{3/2}} \sum_{i=1}^j \frac{\sigma_i \sqrt{1 - \sigma_{i+1}}}{s_i}. \quad (4.22)$$

For $j > j_*$, (where j_* is equal, say, 3) one can take in Eq. (4.22) $\sigma_j = 2s_j \ll 1$. One concludes, that in the inertial interval the PM-velocities decrease linearly in j :

$$V_j = V_0 + \Delta - \frac{2\sqrt{2}\alpha j}{d^{3/2}}, \quad j > j_*, \quad (4.23a)$$

$$\Delta = \frac{\sqrt{2}\alpha}{d^{3/2}} \sum_{i=1}^{\infty} \left[2 - \frac{\sigma_i \sqrt{1 - \sigma_{i+1}}}{s_i} \right]. \quad (4.23b)$$

Here the geometry dependent constant Δ was found by comparison of Eqs. (4.22) and (4.23), and for different geometries it evaluates to:

$$\Delta \approx \frac{\alpha}{d^{3/2}} \times \begin{cases} 2.7, & \text{channel,} \\ 2.4, & \text{pipe.} \end{cases} \quad (4.24)$$

The equation (4.23) can be directly obtained from the condition of the constancy of the momentum flux (3.12), that gives:

$$u_j = \sqrt{2/d} = \text{const.} \quad (4.25)$$

Then, in the stationary case, Eq. (4.20b) determines the j -independent difference $V_j - V_{j+1}$, necessary for keeping the amplitudes of the near-wall eddies at the constant level. This agrees with Eq. (4.23).

In the derivation of Eqs. (4.22) and (4.23) we cancelled in Eq. (4.19b) $u_j = u_j^*$, assuming that $u_j \neq 0$. At a given $\mathcal{R}e$ this assumption is valid only for $j \leq j_0$. Here j_0 is the zone index of the last unstable zone, for which in Eq. (4.20b) $d(\ln u_j)/dt > 0$ at $u_j \rightarrow 0$. To find j_0 we consider Eq. (4.20b) as an equation for a continuous index q and set its RHS to zero with $u_q = 0$:

$$\frac{g\kappa_q}{\mathcal{R}e} = \frac{d}{2}(V_q - V_{q+1}) = \frac{\sqrt{2}\alpha}{\sqrt{d}} \Rightarrow \quad (4.26a)$$

$$q(\mathcal{R}e) = \log_2 \mathcal{R}e + \log_2 \left[2\sqrt{2}\alpha s/g\sqrt{d} \right]. \quad (4.26b)$$

The index j_0 is then the integer part of q .

The solution Eq. (4.22) has still an unknown constant, V_0 . This constant can be found from the stationarity condition (3.12),

$$\mathfrak{p}^- = \sum_{j=1}^{\infty} s_j \Gamma_j V'_j = \mathfrak{p}^+ = 1, \quad (4.27)$$

requiring that the total influx of the linear momentum, caused by the pressure gradient, must dissipate at the wall, due to the viscous friction. The product $s_j \Gamma_j \sim 2^j/\mathcal{R}e$. Therefore, the sum in Eq. (4.27) is dominated by last few terms with $j \approx j_0 \gg j_*$. This allows one to use a more simple Eq. (4.23) instead of Eq. (4.22):

$$1 = \frac{G}{4\mathcal{R}e s} \sum_{j=1}^{j_0} 2^j \left[V_0 + \Delta - \frac{2\sqrt{2}\alpha j}{d^{3/2}} \right] \quad (4.28a)$$

$$\approx \frac{G}{2\mathcal{R}e s} 2^{j_0} \left[V_0 + \Delta - \frac{2\sqrt{2}\alpha j_0}{d^{3/2}} \right] \quad (4.28b)$$

$$\approx \frac{\sqrt{2}\alpha G}{\sqrt{d} g} \left\{ V_0 + \Delta - \frac{2\sqrt{2}\alpha q(\mathcal{R}e)}{d^{3/2}} \right\}. \quad (4.28c)$$

Together with Eq. (4.23a) this gives the dependence of V_j on j for the near wall region, that is *geometry independent*:

$$V_j = \frac{2\sqrt{2}\alpha}{d^{3/2}} [q(\mathcal{R}e) - j] + \frac{\sqrt{d}}{\sqrt{2}\alpha G} g, \quad j > 3. \quad (4.29)$$

The only $\mathcal{R}e$ -dependent factor here is the position of the viscous cutoff $q(\mathcal{R}e)$, given by the Eq. (4.26b). Counting j from $q(\mathcal{R}e)$, one has $\mathcal{R}e$ independent *PM*-velocities. In the physical space this corresponds to the *universality of the TBL profile* measured in the “wall units” $y^+ = y\mathcal{R}e$.

Notice, that in the derivation of Eq. (4.22), we neglected in Eq. (4.20b) the viscous damping term, $g\kappa_j^2/\mathcal{R}e$, with respect to the turbulent one, $\alpha|u_j|\kappa_j$. This approximation fails near the viscous cutoff, because $g\kappa_j/\mathcal{R}e \propto 2^j$ increases exponentially toward large j , while $\alpha|u_j|$ is approximately constant. More detailed analysis shows, that Eq. (4.22) fails only for last two j before the cutoff and instead of sharp cutoff at $j = j_0$ there is a soft decrease of V_j in two zones near $j = j_0$, see Fig. 8.

One can easily see, that the linear in j set of zone velocities (4.29) in the inertial interval corresponds to the log-profile of the mean velocity in the physical space: $V(y) \sim \ln(y\mathcal{R}e/L)$. Actually, by a direct calculation one shows, that the log-profile

$$V^{\log}(y) = \frac{1}{\kappa_{\kappa}} \ln \left(\frac{y\mathcal{R}e}{L} \right) + B, \quad (4.30)$$

corresponds to the zone velocities

$$\begin{aligned} V_j^{\log} &= \frac{\ln 2}{\kappa_{\kappa}} (\log_2 \mathcal{R}e - j) + \left(B - \frac{1 + \gamma_{\text{E}} - \ln(4/\pi)}{\kappa_{\kappa}} \right) \\ &\simeq \frac{0.69}{\kappa_{\kappa}} (\log_2 \mathcal{R}e - j) + B - \frac{1.34}{\kappa_{\kappa}}, \end{aligned} \quad (4.31)$$

where $\gamma_{\text{E}} \simeq 0.58$ is the Euler gamma constant.

Thus, the MZS model describes the transition to the universal log-profile with the von-Karman constant

$$\kappa_{\kappa} = \frac{\ln 2}{2\sqrt{2}} \frac{d^{3/2}}{\alpha} \simeq 0.25 \frac{d^{3/2}}{\alpha}. \quad (4.32)$$

D. Numerical analysis of the turbulent channel flow in the MSZ-model

This Section is devoted to the numerical analysis of the MZS-model of the channel flow in the effective turbulent damping approximation, Eq. (4.19). For simplicity we adopt $g_j = G_j$. *PM*-damping factor G_j was found according to Eq. (2.29) as the matrix elements of the viscous operator on the real part of the *PM*-basis $\Phi'_j(y)$. This gives

$$G_j = 2^{j+2} s_j.$$

Parameters $d = 4.6 \times 10^{-2}$ and $\alpha = 5.9 \times 10^{-3}$ were chosen to reproduce the experimental values of the universal constants $\kappa_{\kappa} \approx 0.4$ and $B \approx 5.2$.

In numerical analysis, 30 zones were sufficient to describe the flows with Reynolds numbers up to 10^9 . In order to find the stationary solution of the full MZS-Eqs. (4.19) we develop extremely stable and efficient iteration procedure, based on the essential physics of the

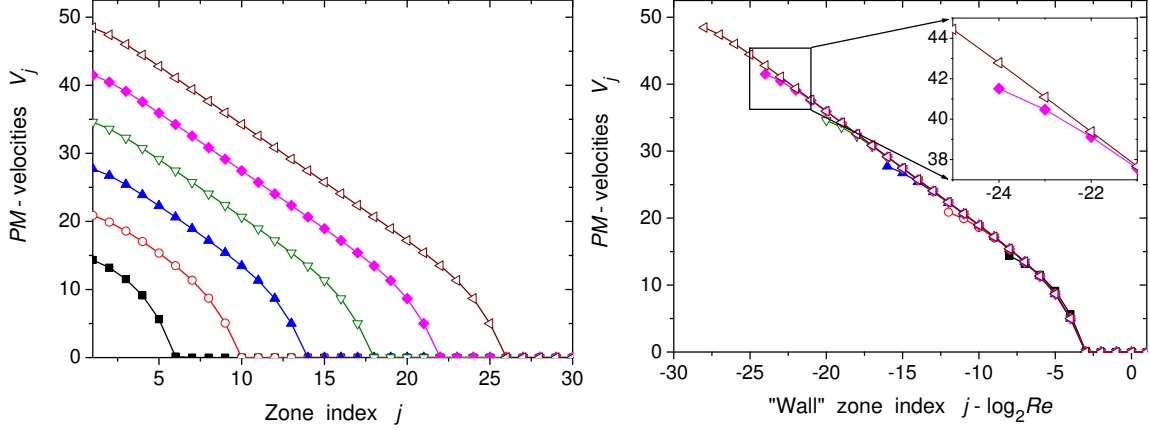


FIG. 8: *PM*-velocities V_j for different Reynolds numbers $\mathcal{R}e$ as a function of the zone index j (left panel) and of the “near-wall” zone index ($j - \log_2 \mathcal{R}e$) (right panel). The lines from lower to upper correspond to $\log_2 \mathcal{R}e = 9, 13, 17, 21, 25$ and 29 , respectively.

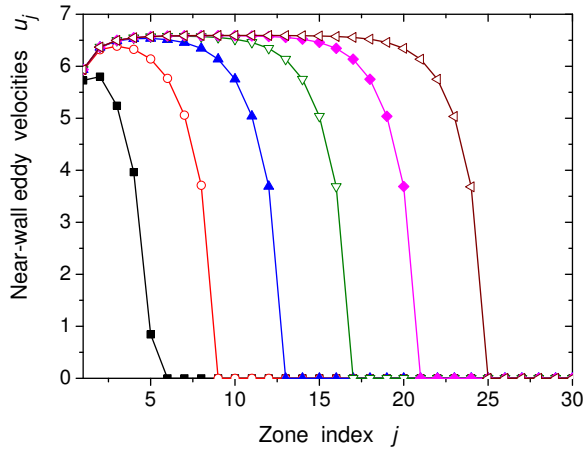


FIG. 9: Magnitude of the near-wall turbulent eddies $|u_j|$ as a function of the zone index j for different $\mathcal{R}e$. The lines are marked as in Fig. 8.

problem, see Appendix B. In spite of the huge Reynolds numbers, the accuracy better than 10^{-6} was reached with about 100-200 iteration. Actually, using our approach (Mzs-model and the iteration procedure) one can simulate turbulent wall-bounded flows for *arbitrary large* $\mathcal{R}e$ with very modest PC, even with XT486@40MHz, 8MB RAM.

1. Behavior of the zone velocities V_j and u_j

In Fig. 8, left panel, we plot *PM*-velocities V_j for different $\mathcal{R}e$ from 500 to 5×10^8 . One clearly sees the inertial

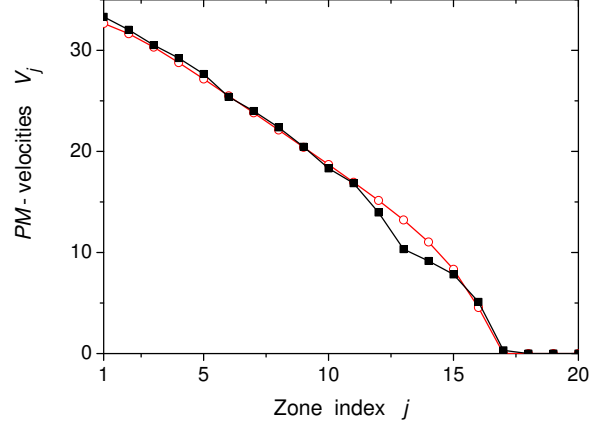


FIG. 10: Comparison of numerical solutions of the full Mzs Eqs. (3.19) [black squares] and Mzs Eqs. (4.19) in the approximation of turbulent viscosity (4.18) [empty circles]. $\mathcal{R}e = 10^6$.

interval, where V_j decrease linearly with j in agreement with Eq. (4.22). As we mentioned above there is a “soft” viscous cutoff, that involves last 2 zones. In order to demonstrate the phenomenon of universality, in the right panel of Fig. 8 we re-plot the same velocities V_j as function of the “near-wall” zone index $j - \log_2 \mathcal{R}e$ as it is suggested by Eq. (4.29). There is a perfect collapse of all lines. Importantly, they collapse not only in the inertial interval, but also in the dissipative cutoff range. There is a non-negligible difference for the first two-three zones, $j = 1, 2$, (see the blow up in the lower panel) that is caused by the non-negligible momentum influx in these zones. This deviation is described by Eq. (4.22).

Fig. 9 shows the magnitudes of the near-wall turbulent eddies, $|u_j|$, for the same set of $\mathcal{R}e$'s. Again, the numerical results are in full agreement with our theoretical understanding: the magnitudes of the near-wall eddies in the inertial interval are constant, as it required by Eq. (4.25) from the condition of the constancy of momentum flux. At the dissipative cutoff we observe a decrease of u_j involving 3–4 zones. A small decrease of u_j at the first few shells is caused by the non-zero momentum flux into these zones; in this region u_j with good accuracy can be found from

$$\mathfrak{p}_j = du_j^2/2 = 1 - \sigma_{j+1}. \quad (4.33)$$

To check how the approximation of turbulent viscosity, Eq. (4.18), affects the resulting mean velocity profile we compare in Fig. 10 the solutions of the full MZS Eqs. (3.19) (black squares) and MZS Eqs. (4.19) in the approximation of turbulent viscosity, Eq. (4.18) (empty circles). These solutions practically coincide except for three zones ($j = 12, 13, 14$) near the viscous cutoff. In these zones just a few shells are excited in the full model (3.19) and the observed difference is an artefact of discreetness of the scale space in the shell models (recall, that in the shell model (3.19) the spacing parameter $\lambda = 2$). In the case when the details of turbulent cascades near the wall are physically important (e.g., in turbulent flows with polymeric additives) one has to use more detailed shell representation of turbulent velocity field, say with $\lambda = \sqrt{2}$ or even $\lambda = 2^{1/4}$, preserving the interaction range in the scale space unchanged. This modification of our model is under construction and will be published elsewhere.

We expect that the more detailed models with $\lambda < 2$ will give the mean profile, closer to that, given by reduced model with turbulent damping (4.19), in which the energy dissipation is affected by the scale spacing. In this paper we are not interested in details of turbulent cascades and will use further only Eqs. (4.19).

2. Reconstruction of the mean velocity profile

The equation (2.14a) reconstructs *PM*-velocity profile $V_{PM}(y)$ from the set of V_j . For the case of the channel flow one has:

$$V_{PM}(y) = \sum_{j=1}^{\infty} V_j \Phi'_j(y), \quad (4.34)$$

$$\Phi'_j(y) = \sum_{m=2^{j-1}}^{2^j-1} p_m \phi_{2m-1}(y),$$

where p_m and $\phi_m(y)$ for the channel geometry are given by Eq. (2.17). The results of such reconstruction for a set of $\mathcal{R}e$'s are shown in Fig. 11. We see that reconstructed *PM*-profiles show all qualitative features of the “real” mean velocity profiles in the well-developed turbulent regime. Namely, the mean *PM*-velocity is almost

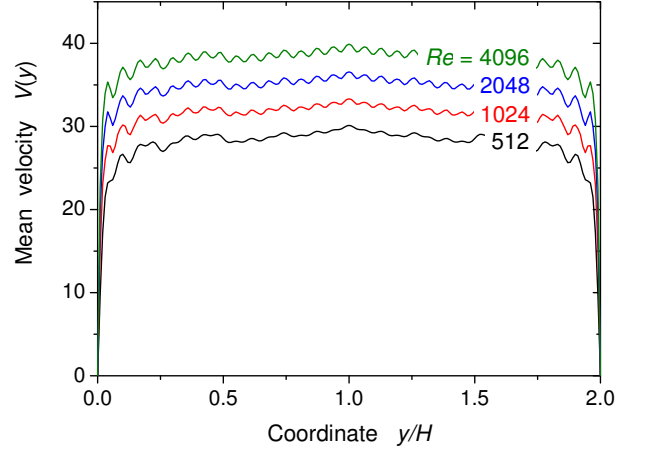


FIG. 11: Reconstructed *PM*-velocity profiles $V_{PM}(y)$ for different Reynolds numbers.

constant in the main part of the flow [with centerline velocity, increasing with $\mathcal{R}e$ as $\ln(\mathcal{R}e)$]. As expected, all fall of $V(y)$ occurs in a small region near the walls. It is also clear, that the width of this near-wall region decreases as $\mathcal{R}e$ increases, in the same way as in real flows.

Figure 11 shows, that the *PM*-profiles have some non-physical “wiggles”. They originate from the incompleteness of the *PM*-basis. Indeed, the *PM*-basis is constructed by Eq. (2.4) from the complete ϕ -basis with some prescribed m -dependence for each j function. As a result, the *PM*-expansion (4.34) can be understood as the Fourier expansion in $\phi_m(y) \propto \sin(k_{2m-1}y)$ with discontinuities of the Fourier amplitudes at the “zone boundaries” $m = 2^j$, which produces the wiggles in the y -representation. This artifact of the model can be removed by different ways. The simplest one is to add some function $\tilde{V}(y)$, orthogonal to all *PM*-basic functions (and thus having zero momentum), with the amplitude and the shape of which are determined from the problem of minimization of discontinuities in the spectrum. It can be shown that the result of such “smoothing” is fully acceptable for the most of purposes.

Figure 12 displays the *PM*-velocities in the near-wall region $y \ll H$ in log-linear scale for different $\mathcal{R}e$'s from $\sim 1.3 \times 10^5$ to $\sim 5 \times 10^8$. The distance from the wall is measured in near-wall viscous lengths, $y^+ = y/\delta = y\mathcal{R}e/H$. The collapse of profiles for different Reynolds numbers is evident. One can see the viscous sublayer (for $y^+ \leq 10$) and universal log-profile (for $y^+ \geq 50$).

3. Comparison of the MZS universal mean velocity profile with experiment and DNS

In Fig. 13 we compared the reconstructed MZS universal mean velocity with the DNS results in chan-

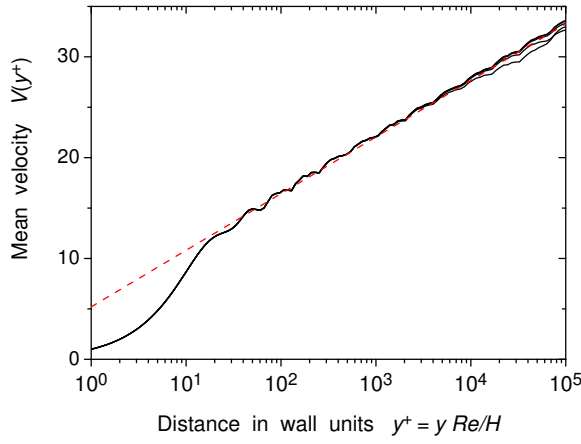


FIG. 12: Collapse of the mean-velocity profiles in the near-wall units. Different line (from below to above) correspond to $\mathcal{R}e = 2^{17} \sim 1.3 \times 10^5, 2^{21}, 2^{25}$ and $2^{29} \sim 5 \times 10^8$

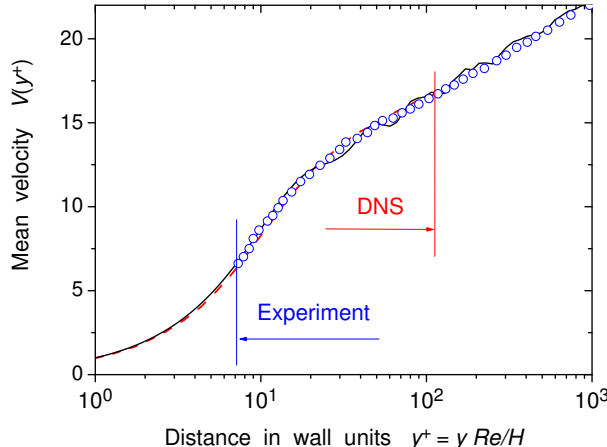


FIG. 13: Comparison of the reconstructed MZS universal mean velocity profile $V(y+)/U_\tau$, (solid line in the region $1 \leq y^+ \leq 10^3$) with the DNS results in channel, available in Ref. [15] for $y^+ < 10^2$ (dashed line) and with the measurements in pipe, taken from Ref. [16] for $y^+ > 10$, (empty circles).

nel, Ref. [15] and with the laboratory measurements at $\mathcal{R}e$ up to 3.5×10^7 , presented in Ref. [16]. The DNS data are available for $y^+ < 100$, while the experimental data are obtained for $y^+ > 10$. As expected, in the overlap region, $10 < y^+ < 100$ both results collapse. As we explained, our MZS model reproduce the asymptotical log-profile (4.30), and the parameters of the model, α and d were chosen to give known values of κ_κ and B , that parameterize Eq. (4.30). Therefore, as expected, the MZS profile, displayed in Fig. 13 as solid line, coincide with the experimental date in the region of large enough y^+ .

The point is that the MZS dependence $V_{PM}(y^+)$ practically coincides with the DNS and experimental data in all region of y^+ . It means that the MZS model correctly describes the basic physics that affect the mean velocity profile in the universal near wall region of turbulent boundary layer near the flat plane. The MZS description of the viscous and the buffer layers *does not require adjustable parameters*.

4. Reconstruction of the profile of the energy dissipation

The total dissipation rate ε_j^- in j -zone, Eq. (3.9a), can be splitted into the dissipation rate in the PM -velocity subsystem $\tilde{\varepsilon}_j^-$ and the dissipation rate in the turbulent subsystem $\hat{\varepsilon}_j^-$:

$$\begin{aligned} \varepsilon_j^- &= \tilde{\varepsilon}_j^- + \hat{\varepsilon}_j^- , \\ \tilde{\varepsilon}_j^- &= \Gamma_j |V_j|^2 , \quad \hat{\varepsilon}_j^- = \sum_{i \leq j} \gamma_{\text{ef},i} |u_i|^2 . \end{aligned} \quad (4.35)$$

In the turbulent viscosity approximation the effective damping is given by

$$\gamma_{\text{ef},j} = \gamma_j + \alpha \kappa_j |u_j| . \quad (4.36)$$

Figure 14 displays as empty circles the dissipation density in turbulent subsystem, normalized by the near-wall lengthscale, i.e. $\hat{\varepsilon}_j^- / \mathcal{R}e$ as a function of the “wall zone number” defined here as

$$j^+ \equiv j - \log_2 \mathcal{R}e + 2 . \quad (4.37)$$

The black squares in this figure show the PM -velocities in the “wall-zone” representation, i.e. values of V_{j+} for the same $\mathcal{R}e = 5 \times 10^8$. The solid line is the log-plot of the reconstructed (from this set of V_j) PM -velocity in the physical space, i.e. $V_{PM}(y^+)$ vs. $\log_2 y^+$, shown from above. As one sees, the solid line goes very close to the black squares, as it should be according to the interpretation of the PM -velocities V_{j+} as a “physical” velocity at some point within j^+ -zone, that explained in Sec. II B 6. As it is clear from Fig. 14, the wall zone numbers (4.37) are chosen to give a very simple “correspondence rule”:

$$\text{Wall zone index } j^+ \Leftrightarrow \text{Wall distance } y^+ = 2^{-j^+} . \quad (4.38)$$

This approach can be used to restore of spatial distribution of various turbulent characteristics. In particular, we can understand ε_{j+}^- , presented in Fig. 14, as $\varepsilon^-(y^+)$ with $y^+ = (2^{-j^+})$. As expected, the dissipation rate (normalized, as in Fig. 14, by $\mathcal{R}e$) is $\mathcal{R}e$ -independent as $\mathcal{R}e \rightarrow \infty$. In this sense, the results in Fig. 14 can be considered as universal. As expected, at large $\mathcal{R}e$ the main energy dissipation occurs in a narrow near-wall region, $y^+ < 40$. The dissipation rate at the wall in our model is equal to

$$\varepsilon|_{\text{wall}} = \lim_{j \rightarrow \infty} \hat{\varepsilon}_j^- / \mathcal{R}e \approx 0.21 , \quad \mathcal{R}e > 10^4 , \quad (4.39)$$

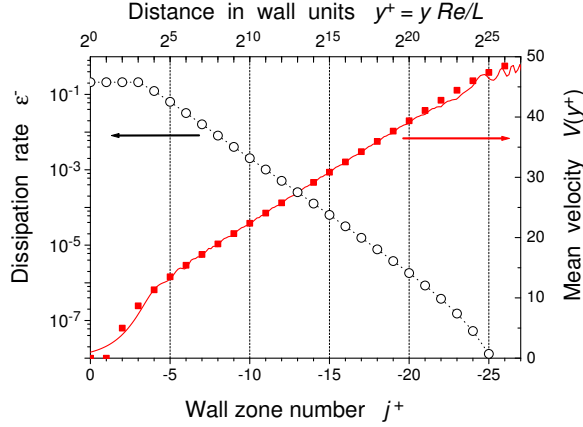


FIG. 14: Mean velocities V_{j+} (black squares) and turbulent dissipation rates ε_{j+}^+ (empty circles) in the wall-zone representation j^+ , introduced by Eq. (4.37). Solid line – reconstruction of the PM-velocity profile (in the wall units) $V_{PM}(y^+)$ vs. distance y^+ in the wall units, shown above. $\mathcal{R}e = 5 \times 10^8$.

which is reasonably close to the result for smaller $\mathcal{R}e$, available in the DNS of Ref. [17]:

$$\varepsilon|_{\text{wall}} = 0.166, \quad \mathcal{R}e \sim 200. \quad (4.40)$$

Notice, the difference in $\mathcal{R}e$'s and that our result (4.39) is obtained in the simple model with just two adjustable parameters, chosen to adjust very different characteristics of the flow, the mean velocity profile. This allows one to consider the reasonable correspondence of Eqs. (4.39) and (4.40) as an argument in favor of our simple MZS model.

5. $\mathcal{R}e$ -dependence of the global flow characteristics

Clearly, our approach allows one to evaluate various global characteristics of the turbulent wall bounded flows.

The first example is the $\mathcal{R}e$ -dependence of the total momentum (i.e. total flux) of the flow, shown in Fig. 15. There is a laminar regime for $\mathcal{R}e < 17$, and a developed turbulent regime for, say $\mathcal{R}e > 100$. The “period-2” oscillations are an artifact of the model, caused by the discretization with the spacing parameter $\lambda = 2$. These oscillations, however, are small and should be ignored. In principle, they can be removed in more “advanced” versions of the MZS models with few variables in each j -zone, $V_{j,\sigma}$, $u_{j,\sigma}$, responsible for “ σ -sub-zones of the j -zone.

The second example is the $\mathcal{R}e$ -dependence of the total energy of the system, as well as parts of the energy, containing in the mean and turbulent subsystems, shown in Fig. 16.

Last, but not least, example is the $\mathcal{R}e$ -dependence of the total energy dissipation and that for the V - and u -

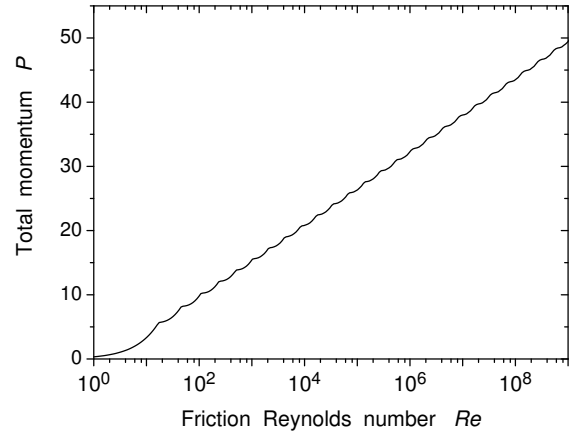


FIG. 15: Dependence of the total momentum of the flow \mathcal{P} from the Reynolds number $\mathcal{R}e$ in the channel flow.

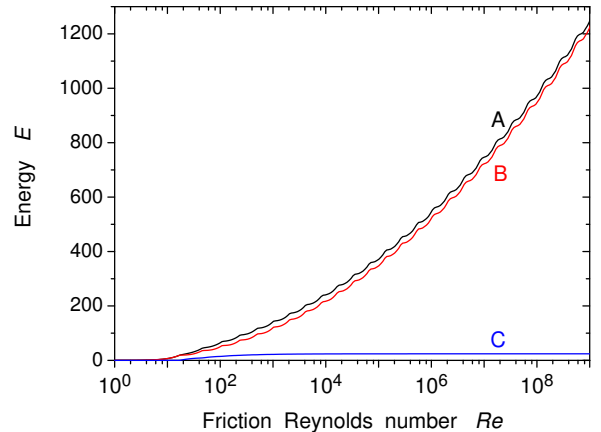


FIG. 16: Dependence of the total energy (A), the energy of the mean V -subsystem (B), and the energy of the turbulent u -subsystem (C) from the Reynolds number $\mathcal{R}e$.

subsystem, shown in Fig. 17. Total energy dissipation is equal to the total energy influx, i.e. to the total momentum of the flow. However, the distribution of energy dissipation between two subsystems is very interesting.

One clearly sees that some flow characteristics, like the energy of turbulent subsystem and the energy dissipation in the mean flow subsystem remain finite for vanishing fluid viscosity, ν_0 . In the same time, other characteristics, such as the total linear momentum, the energy of the mean flow sub-system and the rate of energy dissipation increase infinitely [like $\ln(1/\nu_0)$], i.e. demonstrate a phenomenon of *viscous anomaly*. The MZS model clearly demonstrate that the physical reason for that anomaly is the separation in the physical space of the external forcing and the friction: the external pressure gradient, that accelerate the flow, acts on the whole cross-section

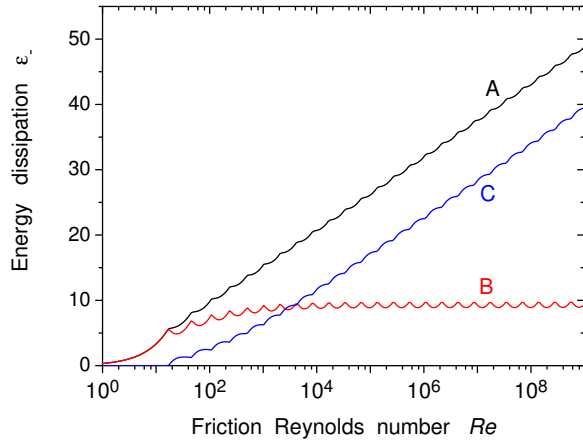


FIG. 17: Dependence of the total energy dissipation (A), energy dissipation in the mean V -subsystem (B), and energy dissipation in the turbulent u -subsystem (C) from the Reynolds number $\mathcal{R}e$.

area of the flow, while the friction force, that prevents the mean velocity from infinite growth, acts only on the walls. To be able to maintain the constant flux of the linear mechanical momentum toward the wall, the amplitudes of the near-wall eddies of all scales, u_j , must be j -independent. This immediately leads to a linear increase of V_j with j , decreasing from the viscous cutoff value, j_0 , toward the beginning of the cascade, $j = 1$. Thus the value of V_1 is proportional to the total number of the cascade steps, $j_0 - 1$. Decrease of ν_0 to a half of its value adds one more step in inertial interval of the momentum cascade. This leads to an increase of V_1 by $\sim \ln 2$. In the dimensional units this corresponds to the increase V_1 by $\sim V_\tau \ln 2 \sim \ln 2 \sqrt{L \nabla p}$.

V. SUMMARY

We develop a multi-zone shell (Mzs) model for the wall-bounded turbulent flows in the piecewise approximation, dividing cross-section area into set of $N \sim \log_2 \mathcal{R}e$ j -zones. In each zone the turbulence is assumed to be homogeneous and is described in the framework of a shell model equation for the “turbulent” shell velocities $u_{nj}(t)$. The mean velocity is described by an additional set of N zone variables $V_j(t)$, that allow to reconstruct the mean velocity profile with the help of a specially designed PM -basis.

The Mzs model

- conserves the actual integrals of motion of the original NSE of the problem, *energy, linear and angular momenta*;
- respects Galilean and “asymptotic” scale invariance, NSE type of nonlinearity.
- in the relatively simple and analytically transparent

manner describes the basic physical phenomena in the wall bounded flows for a huge interval of Reynolds numbers. They include:

1. the laminar velocity profile for $\mathcal{R}e < \mathcal{R}e_{cr}$;
2. its instability at $\mathcal{R}e = \mathcal{R}e_{cr}$,
3. intermediate, non-universal mean velocity profile at moderate $\mathcal{R}e$;
4. universal profile for $\mathcal{R}e \gg \mathcal{R}e_{cr}$ in the viscous sub-layer, buffer layer and log-law region;
5. spatial distribution of turbulent activity, of the rate of energy dissipations, *etc.*

- allows additional adaptation of the Mzs equations for first few (energy containing) shells to the particular flow geometries (like the channel, pipe, Couette flows, *etc.*) that may be based on the stability analysis of the laminar regime or some other specific geometry determined information. This should improve description of the flow for moderate $\mathcal{R}e < 1000$.
- may be generalized on the case of viscoelastic turbulent flows (by adding additional shell variables for the polymeric additives), on the case of particle laden suspensions, etc.

Acknowledgments

We thank Itamar Procaccia, Nikolai Nikitin and Alex Yakhot for useful discussions. The support of the Israel Science Foundation governed by the Israeli Academy of Science is gratefully acknowledged.

APPENDIX A: EQUATION FOR THE LAMINAR PM -PROFILE

Here we present a proof that the laminar PM -profile, $\mathbf{V}_{PM}^0(\rho)$, given by Eq. (4.2), satisfies Eq. (4.4).

To this end, we recall that the damping parameters $G_j \kappa_j^2$ are defined as matrix elements:

$$G_j \kappa_j^2 = -s_j^{-1} (\Phi'_j, \Delta \Phi'_j). \quad (A1)$$

Substituting this definition into (4.1), (4.2), we obtain

$$\mathbf{V}_{PM}^0(\rho) = -\mathcal{R}e \sum_j \frac{s_j \Phi'_j(\rho)}{(\Phi'_j, \Delta \Phi'_j)}. \quad (A2)$$

Then, the Laplacian of \mathbf{V}_{PM}^0 is equal to

$$\Delta \mathbf{V}_{PM}^0(\rho) = -\mathcal{R}e \sum_j \frac{s_j \Delta \Phi'_j(\rho)}{(\Phi'_j, \Delta \Phi'_j)}. \quad (A3)$$

Acting on this Laplacian with the *PM*-projector (2.12), we obtain

$$\hat{P}_{PM}\{\Delta V_{PM}^0\} = -\mathcal{R}e \sum_{jk} \frac{s_j}{s_k} \operatorname{Re} \left\{ \Phi_k \frac{(\Phi_k \Delta \Phi'_j)}{(\Phi'_j, \Delta \Phi'_j)} \right\}, \quad (\text{A4})$$

where one must distinguish the Reynolds number, $\mathcal{R}e$, from the notation of the real part of something, $\operatorname{Re}\{\dots\}$. Note that by construction, different *PM*-functions Φ_j belong to the different subspaces of the eigen-functions of the Laplace operator. Also, the real Φ'_j and imaginary Φ''_j parts of these functions are orthogonal, and thus

$$(\Phi_k, \Delta \Phi'_j) = \Delta_{kj} (\Phi'_j, \Delta \Phi'_j). \quad (\text{A5})$$

As a result, all non-diagonal terms in (A4) vanish, and we obtain

$$\hat{P}_{PM}\{\Delta V_{PM}^0\} = -\mathcal{R}e \sum_j \Phi'_j. \quad (\text{A6})$$

Finally, using property (2.11a), we obtain

$$\hat{P}_{PM}\{\Delta V_{PM}^0\} = -\mathcal{R}e \hat{x}, \quad (\text{A7})$$

which actually is Eq. (4.4).

APPENDIX B: ITERATION PROCEDURE FOR SOLVING MZS EQUATIONS IN THE EFFECTIVE TURBULENT DAMPING APPROXIMATION

Consider the MZS-Eqs.(4.19) for some large $\mathcal{R}e$. As we discussed, there are two regions of j , namely $j < j_{\max}$ and $j \geq j_{\max}$. In the “turbulent region”, $j < j_{\max}$, the laminar solution, $u_j = 0$, is unstable with respect to excitation of turbulent amplitudes u_j and thus, in the stationary regime, $u_j \neq 0$. For $d > 0$, without loss of generality all u_j can be taken real and positive definite. In the turbulent region the stationary velocities V_j and u_j satisfy the equation:

$$\Gamma_j V_j = 1 + d \kappa_j (u_{j-1}^2 - u_j^2), \quad (\text{B1a})$$

$$\gamma_j + \alpha \kappa_j u_j = \frac{d}{2\sigma_j} (V_j - V_{j+1}), \quad (\text{B1b})$$

$$u_j \geq 0, \quad j < j_{\max}.$$

In the “laminar region”, $j \geq j_{\max}$:

$$V_j = 1/\Gamma_j, \quad u_j = 0, \quad j \geq j_{\max}. \quad (\text{B2})$$

One can substitute V_j from Eq. (B1a) to Eq. (B1b) and get an equation, connecting the triad u_{j-1} , u_j , and u_{j+1} . Unfortunately, a direct iteration procedure in this “straightforward” equation is unstable and do not converge to the stationary solution.

To find the stable, stationary solution of Eqs. (B1) numerically, we develop a stable iteration procedure, which is based on the physical understanding of these equations as describing the momentum flux from $j = 1$ toward large j in the “interaction triads” V_j , V_{j+1} and u_j . Denote as $V_j^{(p)}$, $\tilde{V}_{j+1}^{(p)}$ and $u_j^{(p)}$ the solution of following three algebraic equations on the j -step in the p -th iteration run:

$$\begin{aligned} \Gamma_j V_j^{(p)} &= 1 + d \kappa_j \{[u_{j-1}^{(p)}]^2 - [u_j^{(p)}]^2\}, \\ \Gamma_{j+1} \tilde{V}_{j+1}^{(p)} &= 1 + d \kappa_{j+1} \{[u_j^{(p)}]^2 - [u_{j+1}^{(p-1)}]^2\}, \\ \gamma_j + \alpha \kappa_j u_j^{(p)} &= \frac{d}{2\sigma_j} [V_j^{(p)} - \tilde{V}_{j+1}^{(p)}], \\ u_j^{(p)} &\geq 0, \quad \text{for } j_{\max} > j \geq 1, \quad u_0^{(p)} = 0. \end{aligned} \quad (\text{B3})$$

As the “initial condition” at $p = 0$ we take the (unstable) laminar solution:

$$V_j^{(0)} = \Gamma_j^{-1}, \quad u_j^{(0)} = 0.$$

In the first step, $j = 1$, of each iteration run one takes $u_0^{(p)} = 0$. Finding $V_1^{(p)}$, $\tilde{V}_2^{(p)}$, and $u_1^{(p)}$ one takes in Eq. (B3) $j = 2$, finds $V_2^{(p)}$, $\tilde{V}_3^{(p)}$ and $u_2^{(p)}$ and so on until on some j_0 step one gets negative (or complex) solution for $u_{j_0}^{(p)}$. It means that this amplitude is stable and has to be taken zero, $u_{j_0}^{(p)} = 0$. Accordingly, $j_0 = j_{\max}$. For all $j > j_{\max}$ one takes the laminar solution: $V_j^{(p)} = 1/\Gamma_j$, $u_j^{(p)} = 0$.

After that one begin the next, $p + 1$, iteration run, starting again from its first step, $j = 1$. It can be shown, that the velocities $V_1^{(p)}$ form monotonically decreasing sequence with increasing p and are always positive. Since a limited from below, monotonically decreasing sequence always have some finite limit, this proves the convergence and stability of our iteration scheme. The calculations show, that for Reynolds numbers $\mathcal{R}e \leq 10^9$ velocities V_j and u_j converge (with accuracy about 10^{-6}) after 100 – 200 iterations runs.

[1] E. B. Gledzer. Dokl. Akad. Nauk. SSSR **200**, 1043, (1973).
[2] M. Yamada and K. Ohkitani. J. Phys. Soc. Jpn. , **56**, 4210, (1987).
[3] V. S. L'vov, E. Podivilov, A. Pomyalov, I. Procaccia and D. Vandembroucq, Phys. Rev. E **58**, 1811 (1998).
[4] Bohr, T., Jensen, M., Paladin, G. and Vulpiani, A. *Dynamical Systems Approach to Turbulence* (Cambridge

University Press, 1998).

- [5] V. Zimin and F. Hussain, *Phys. Fluids*, **7** 2925, (1995).
- [6] P. Frick and V. Zimin, "Hierarchical models of turbulence", in *Wavelets Fractals and Fourier Transforms* (Clarendon, Oxford, 1993).
- [7] C. Meneveau, *J. Fluid Mech.* **232** 469 (1991).
- [8] S.B. Pope, *Turbulent flows* (Cambridge Univ. Press, Cambridge, 2000).
- [9] J. L. Lumley, *Adv. Appl. Mech.* **18**, 123 (1978).
- [10] A.S. Monin and A.M. Yaglom, *Statistical Fluid mechanics of turbulence* (MIT Press, Cambridge, MA, 1975), vol. 2
- [11] V. Yakhot and S. A. Orszag, *J. Sci. Comput.*, **1** 3 (1986),
- [12] V. Yakhot, S.A. Orszag, S. Thangam, T.B. Gatski, and C. G. Speziale, *Phys. Pluids A* **4** 1510 (1992).
- [13] L. M. Smith and W. C. Reynolds, *Phys. Fluids A* **4** 364 (1992).
- [14] M. Holschneider, *Wavelets, an analysis tool*, (Clarendon, Oxford, 1995).
- [15] E. De Angelis, C. M. Casciola, V.S. L'vov, R. Piva, and I. Procaccia, *Phys. Rev. E.*, **67**, #5 (2003).
- [16] M.V. Zagarola and A.J.Smits, *Phys. Rev. Lett.*, **78**, 239 (1997).
- [17] N.N. Mansour, J. Kim, and P. Moin, *J. Fluid Mech.*, **194**, 15 (1998).